A fluorescent sensor for spatiotemporally resolved endocannabinoid dynamics *in vitro* and *in vivo*

Ao Dong[1,2,3], Kaikai He[1,2], Barna Dudok[4], Jordan S Farrell[4], Wuqiang Guan[5], Daniel J Liput[6,7], Henry L Puhl[7], Ruyi Cai[1,2], Jiali Duan[1,2], Eddy Albarran[8], Jun Ding[9], David M Lovinger[6], Bo Li[5], Ivan Soltesz[4], & Yulong Li[1,2,3,10,*]

[1]State Key Laboratory of Membrane Biology, Peking University School of Life Sciences, Beijing, China;
[2]PKU-IDG/McGovern Institute for Brain Research, Beijing, China;
[3]Peking-Tsinghua Center for Life Sciences, Academy for Advanced Interdisciplinary Studies, Peking University, Beijing, China;
[4]Department of Neurosurgery, Stanford University, Palo Alto, CA, USA;
[5]Cold Spring Harbor Laboratory, Cold Spring Harbor, NY, USA;
[6]Laboratory for Integrative Neuroscience, National Institute on Alcohol Abuse and Alcoholism, Bethesda, MD, USA;
[7]Laboratory of Molecular Physiology, National Institute on Alcohol Abuse and Alcoholism, Bethesda, MD, USA;
[8]Neuroscience PhD Program, Stanford University, Palo Alto, CA, USA;
[9]Department of Neurosurgery, Department of Neurology, Stanford University School of Medicine, Palo Alto, CA, USA;
[10]Chinese Institute for Brain Research, Beijing, China.

*Correspondence should be addressed to Y.L. (yulongli@pku.edu.cn).

Endocannabinoids (eCBs) are retrograde lipid neuromodulators involved in many physiologically important processes. However, their release and dynamics in the brain remain largely unknown, in part due to lack of probes capable of reporting real-time eCBs with sufficient spatiotemporal resolution. Here, we developed a new G protein-coupled receptor Activation Based eCB sensor GRAB$_{eCB2.0}$ using the human CB1 cannabinoid receptor and a circular-permutated EGFP. GRAB$_{eCB2.0}$ exhibited proper cell membrane trafficking, ~seconds kinetics, high specificity and robust fluorescence response to eCBs at physiological concentrations. Using GRAB$_{eCB2.0}$, we detected evoked eCB dynamics in both cultured neurons and acute brain slices. Interestingly, we also observed spontaneous compartmental eCB transients that spread ~11 μm in cultured neurons, suggesting locally-restricted eCB signaling. By expressing GRAB$_{eCB2.0}$ *in vivo*, we readily observed foot-shock elicited and running triggered eCB transients in mouse amygdala and hippocampus, respectively. Lastly, using GRAB$_{eCB2.0}$ in an epilepsy model, we observed a spreading eCB wave following a calcium wave in mouse hippocampus. In summary, GRAB$_{eCB2.0}$ is a powerful new probe to resolve eCB release and dynamics under both physiological and pathological conditions.

Cannabis derivatives have long been used for medicinal and recreational purposes across

cultures in formulations such as marijuana and hashish[1]. Bioactive compounds in cannabis, phytocannabinoids, exert their function by hijacking the endocannabinoid system in our body. The biological function of endocannabinoids (eCBs), majorly two lipid metabolites 2-arachidonoylglycerol (2-AG) and anandamide (AEA), is primarily mediated by the activation of two G protein-coupled receptors (GPCRs), cannabinoid receptor type 1 (CB1R) and type 2 (CB2R)[2]. As important neuromodulators, eCBs are widely distributed in the peripheral and central nervous system. Interestingly, distinct from other classical neurotransmitters that are stored in synaptic vesicles and released from presynaptic terminals, eCBs are typically produced and released from the postsynaptic site in a neuronal activity-dependent manner, then retrogradely travel to the presynaptic terminal and activate the CB1R, activation of which often results in an inhibition of presynaptic neurotransmitter release[3,4]. In addition, eCBs can also function in glial cells and intracellular organelles[5-9]. eCBs participate in the short-term and long-term synaptic plasticity of glutamatergic and gamma-aminobutyric acid (GABA)-ergic synapses in a variety of brain regions such as cerebral cortex, hippocampus, striatum, ventral tegmental area, amygdala and cerebellum[4,10], and play important roles in many physiological processes including development, emotional state, pain, sleep/wake cycle, energy metabolism, reward, learning and memory[11-15]. Given the broad distribution and functions of eCBs, dysregulation of eCB system is tightly linked with a variety of disorders, including neuropsychiatric and neurodegenerative diseases, epilepsy, cancer, and others[16-18]. Therefore, the eCB system has become a therapeutic target for treating multiple neurological diseases[19,20].

In contrast to the increasing knowledge about the eCB biochemistry and physiology, the spatiotemporal dynamics of eCBs in the brain remains largely unknown. Synaptic transmission mediated by classic neurotransmitters such as glutamate and GABA and their ionotropic receptors can happen in milliseconds timescale and is confined to the nanometer dimensions of the synaptic cleft[21], while neuropeptides are thought to be secreted in seconds or minutes after stimulation and act at longer distances[22]. However, our understanding of eCB signaling is limited due to drawbacks of existing eCB detection methods. For example, qualitative and quantitative measurement of eCBs in brain tissues can provide valuable information on eCB levels. However, this usually relies on lipid extraction, purification and analysis by chromatography and mass spectrometry[23,24], therefore, has poor spatial and temporal resolution and cannot detect eCBs *in vivo*. Electrophysiology, together with genetics and pharmacology, is frequently used to provide indirect measurement of eCB action by studying eCB-mediated synaptic modulation[25-28]. However, this method is mostly used in *in vitro* preparations with reduced physiological relevance and has poor spatial resolution. Microdialysis, while challenging for hydrophobic lipid molecules, has been used to monitor eCB abundance in the brain during pharmacological manipulations and behaviors[29,30], but it has a long sampling interval (~minutes) that is well beyond the time scale of synaptic plasticity mediated by eCBs (~sub-second to seconds), preventing the accurate detection of eCBs in real time *in vivo*. Therefore, development of an *in vivo* eCB detection tool with satisfactory spatiotemporal resolution would meet a clear need in this field.

Recently, several GPCR- and circular-permutated (cp) fluorescent protein-based

sensors for neurotransmitters and neuromodulators were successfully developed[31-39]. Following this strategy, here we report a novel GPCR Activation Based eCB sensor $GRAB_{eCB2.0}$ (eCB2.0 for simplicity) based on the human CB1R and cpEGFP. eCB2.0 exhibits proper membrane trafficking, high specificity, ~second-scale kinetics, ~800% fluorescence response to 2-AG and ~550% to AEA in cultured neurons. After validating the performance of eCB2.0 in cultured cells and acute brain slices, we are able to detected foot-shock evoked eCB signals in the amygdala in freely moving mice and eCB dynamics in the mouse hippocampus during running and seizures.

RESULTS

Development and *in vitro* characterization of $GRAB_{eCB}$ sensors

Among the two cannabinoid receptors, we chose CB1R as the eCB sensor scaffold, because it has a higher affinity towards eCBs than CB2R[40]. To start, we inserted the intracellular loop 3 (ICL3)-cpEGFP module from our recently developed $GRAB_{NE}$ sensor[34] into the ICL3 of human CB1R (**Fig. 1a**). After several rounds of screening for insertion site and $GRAB_{NE}$ ICL3 truncation, we generated the first generation eCB sensor named $GRAB_{eCB1.0}$ (eCB1.0 for simplicity), which showed a moderate response ($\Delta F/F_0$ ~100%) and 3 μM apparent affinity for 2-AG (**Fig. 1b and Extended Data Fig. 1a**). To further improve the dynamic range of the eCB sensor, we selected 8 sites in cpEGFP for individual random mutation based our the experience gained through the development of previous GRAB sensors[31,33-35,37-39] (**Extended Data Fig. 1b**). A combination of mutations from single-mutation candidates with improved performance resulted in $GRAB_{eCB1.5}$ (eCB1.5), which showed a higher response ($\Delta F/F_0$ ~200%) than eCB1.0 (**Extended Data Fig. 1a**). We next focused on the CB1R ligand binding pocket, aiming to further improve the response and affinity of the sensor. Residues $F177^{2.64}$, $V196^{3.32}$ and $S383^{7.39}$ were selected for targeted screening based on studies of CB1R structure[41-46] (**Extended Data Fig. 1c**). Interestingly, we found that eCB1.5 $S383^{7.39}T$ showed an increased response and a similar apparent affinity to 2-AG compared to eCB1.5, while eCB1.5 $S383^{7.39}T$ $F177^{2.64}A$ showed no response to 2-AG (**Extended Data Fig. 1a**). We thus named eCB1.5 $S383^{7.39}T$ as $GRAB_{eCB2.0}$ (eCB2.0), and eCB1.5 $S383^{7.39}T$ $F177^{2.64}A$ as $GRAB_{eCBmut}$ (eCBmut) (**Extended Data Fig. 2**), which is an eCB non-binding mutant sensor to be used as a negative control.

Both eCB2.0 and eCBmut exhibited proper cell membrane trafficking when expressed in HEK293T cells (**Fig. 1c**). Upon application of ligands, eCB2.0 showed concentration-dependent fluorescence increases to both 2-AG and AEA, with the maximum $\Delta F/F_0$ ~210%, and half maximal effective concentrations (EC_{50}) of ~7.2 μM for 2-AG and ~0.5 μM for AEA. On the contrary, eCBmut showed no response to 2-AG or AEA at all concentrations tested (**Fig. 1d**). We then tested whether eCB2.0 signal was specific to eCBs but not other neurotransmitters. eCB2.0 responses to 10 μM 2-AG and AEA were completely blocked by the CB1R inverse agonist AM251 (10 μM), and eCB2.0 showed no response to other common neurotransmitters or neuromodulators (**Fig. 1e**). Next, we measured the kinetics of eCB2.0 by local micropressure (puff) application (**Fig. 1f**). HEK293T cells expressing eCB2.0 were exposed to puffs of 100 μM 2-AG to measure the "on" kinetics, and cells expressing eCB2.0 and incubated in 10 μM 2-AG were exposed to

puffs of 100 μM AM251 to measure the "off" kinetics at room temperature. Time constants of on and off kinetics were ~1.6 s and ~11.2 s, respectively (**Fig. 1g**). To examine whether or not there is any potential downstream coupling of eCB sensors with intracellular signaling pathways, we first measured G-protein activation using a $G_{\beta\gamma}$ BRET sensor based on the $G_{\beta\gamma}$ binding region of phosducin fused to NanoLuc luciferase. This unified BRET sensor was based upon similar systems[47,48]. 20 μM 2-AG significantly increased the BRET signal in wild-type CB1R expressing cells, indicating that G-protein signaling was activated, but not in cells expressing eCB2.0, eCBmut or in blank control cells (**Fig. 1h**). We then measured β-arrestin recruitment using the Tango assay[49]. We found that AEA potently recruited β-arrestin in CB1R expressing cells but not in either eCB2.0, eCBmut or blank control cells (**Fig. 1i**). These data together demonstrate that eCB2.0 and eCBmut have no detectable coupling with the two main GPCR downstream effectors, implying that the expression and activation of eCB sensors themselves may have minimal perturbation to cell physiology.

To examine the performance of eCB sensors in neurons, we first sparsely expressed eCB2.0 in cultured rat cortical neurons. We found eCB2.0 targeted to the cell membrane throughout the neuron, including axons and dendrites, as indicated by the colocalization of eCB2.0 with the axonal presynaptic marker synaptophysin-mScarlet and the postsynaptic marker PSD95-mScarlet, respectively (**Fig. 2a**). To measure the response of eCB sensors, we infected cultured rat cortical neurons by adeno-associated viruses (AAVs) carrying eCB2.0 and eCBmut under the control of the human synapsin promoter, which enables efficient labeling of all neurons in the culture. eCB2.0 showed fluorescence responses to bath-applied 2-AG and AEA in a concentration-dependent manner. In contrast, eCBmut showed no response to 2-AG or AEA (**Fig. 2b,c**). The maximum responses of eCB2.0 to 2-AG and AEA were ~800% and 550%, and EC_{50}s were ~17.2 μM and ~0.7 μM, respectively. eCB2.0 responses in neurites were higher than in somata (**Fig. 2d**). Bath application of the CB1R agonist WIN55212-2, which can activate eCB2.0 (**Extended Data Fig. 3a**), induced a fluorescence increase of eCB2.0 on neuronal membrane that was stable for as long as 2 hours (**Fig. 2e**). These results indicate minimal arrestin-mediated internalization or desensitization of eCB2.0 sensor in neurons, suggesting the utility of the sensor for long-term eCB imaging.

Imaging endogenous eCBs in primary cultured neurons using eCB2.0

Cultured neurons are commonly used for studying eCB mediated synaptic modulation[28,50]. Thus, we examined whether eCB2.0 can detect endogenous eCB release from primary rat cortical neurons. Firstly, we expressed eCB2.0 and a red glutamate sensor R^{ncp}-iGluSnFR[51] in neurons using AAVs to simultaneously record eCB and glutamate dynamics. Electrical field stimulation (100 pulses at 50 Hz) elicited robust eCB and glutamate signal increases (**Fig. 3a**), demonstrating that eCB2.0 is able to report endogenous eCB release and can be used together with red indicators. We then expressed eCB2.0 in neurons using AAVs and loaded neurons with red calcium dye Calbryte590 to simultaneously record eCBs and neuronal calcium activity. Again, 100 pulses at 50 Hz elicited strong calcium and eCB signals (**Fig. 3b**). The rise and decay kinetics of the calcium signal were faster than those of the eCB signal, consistent with the notion that eCB production is dependent on

calcium[52]. When we stimulated neurons by 1, 5, 10 and 20 pulses at 20 Hz, we observed progressively increased peak calcium and eCB signals. The peak eCB and peak calcium signals were highly correlated (R^2 = 0.99, **Fig. 3c**). Importantly, when we removed calcium from the extracellular solution, a 20-pulse-stimulation was unable to elicit either calcium or eCB signal (**Fig. 3c**), confirming the requirement of calcium activity on eCB release.

Next, we asked which specific eCB(s), namely, 2-AG and/or AEA, was released in cultured rat cortical neurons. 2-AG is mainly produced from diacylglycerol (DAG) by diacylglycerol lipase (DAGL) in postsynaptic neurons (**Fig. 3d**). After applying DO34, a potent and selective DAGL inhibitor[53], the electrically evoked eCB signals were gradually decreased and were almost abolished after 30 min incubation (**Fig. 3e,f**), indicating 2-AG is mobilized via DAGL in cultured neurons. We further validated this by manipulating the eCB degradation pathways: JZL184, an inhibitor of the main 2-AG degrading enzyme monoacylglycerol lipase (MAGL)[54], significantly prolonged the decay phase of evoked eCB signals (**Fig. 3g-i**); in contrast, URB597, an inhibitor of the main AEA degrading enzyme fatty acid amide hydrolase (FAAH)[55], only slightly increased the decay time constant. These data together demonstrate that 2-AG, but not AEA, is the major eCB released from cultured rat cortical neurons in response to trains of electrical stimulation.

In addition to the stimuli-evoked eCB signals, we also observed spontaneous, local eCB transients in neurons in the absence of external stimulation (**Fig. 3j**). The amplitude and rise kinetics of the transient eCB signal were smaller and slower than that of a single-pulse evoked eCB signal from the same region of interest (ROI) (**Fig. 3k,l**), suggesting different releasing patterns of eCBs in these two conditions. The diameter of the transient signal was ~11.3 μm quantified by the full width at half maximum (FWHM) (**Fig. 3m**), consistent with previous speculations that eCB functions in local compartments[56,57]. These spontaneous transients were specific because no such transients were observed in the presence of AM251 (**Fig. 3l,n,o**).

Validation of eCB2.0 in acute mouse brain slices

To further test the ability of eCB2.0 to detect endogenous eCBs in more physiological relevant conditions, we next expressed eCB sensors in acute mouse brain slices. We first injected AAVs carrying eCB2.0 or eCBmut into mouse dorsolateral striatum (DLS, **Fig. 4a**), where eCBs mediate short- and long-term depression and regulates motor behavior[58-60]. Four weeks after AAV injection, acute brain slices were prepared and the expression of eCB sensors could be visualized (**Fig. 4b**). The fluorescence signals evoked by electrical stimuli in the DLS was recorded by photometry. Two-pulse stimulation was sufficient to elicit robust fluorescence increases in a stimulation frequency-dependent manner, while 5- and 10-pulse stimuli elicited even larger signals (**Fig. 4c,d**). The rise and decay kinetics of eCB2.0 signals were ~0.8–1.2 s and ~5.2–8.5 s respectively, as quantified by half rise time and decay time constant (**Fig. 4d**). When we pre-treated brain slices with 10 μM AM251, the same electrical stimuli failed to evoke an eCB2.0 signal change, indicating the eCB signals were specific (**Fig. 4e**). eCBmut showed no response to electrical stimuli, further demonstrating the signal specificity (**Fig. 4e**). 2-photon (2P) microscopic images of eCB2.0 in striatal slices showed the expression of eCB2.0 and its response to bath-applied AEA (**Extended Data Fig. 4**). We also expressed the eCB2.0 in mouse hippocampal CA1 region,

where eCBs modulate both excitatory and inhibitory inputs[61,62], and recorded eCB2.0 signal in acute slices using 2P microscopy (**Fig. 4f,g**). Electrical stimuli from 5 pulses to 100 pulses at 20 Hz evoked eCB2.0 fluorescence increases (**Fig. 4g,h**), similar to the results in DLS. Perfusion of 10 μM AEA to the hippocampal slice evoked a large signal increase, which was blocked by further perfusion of 10 μM AM251 (**Fig. 4i**). In the presence AM251, even 100 pulses no longer elicited eCB2.0 signal (**Fig. 4j**). These data together demonstrate that eCB2.0 can be used to detect endogenously released eCBs in acute brain slices with high sensitivity, specificity and spatiotemporal resolution.

Detection of eCBs in basolateral amygdala during foot shock in freely moving mice

Basolateral amygdala (BLA) is a key brain region mediating fear responses and processing aversive memories[63]. Previous studies demonstrated that the CB1R is highly expressed in the BLA, and the eCB system in BLA participates in stress expression[64-66]. To directly record eCB dynamics in animals during an aversive stimulus, we co-expressed eCB2.0 (or eCBmut) and mCherry in mouse BLA using AAVs and conducted local fiber photometry recordings (**Fig. 5a,b**). A 2-s electrical foot-shock stimulus induced a time-locked eCB2.0 signal increase in the BLA (**Fig. 5c**), and the response was reproducible in 5 consecutive trials (**Fig. 5d**). As negative controls, mCherry and eCBmut showed no fluorescence change during the foot shock (**Fig. 5c,e**). The rise and decay kinetics of eCB2.0 signal were ~1.0 s and ~6.3 s respectively (**Fig. 5f**). Taken together, these data demonstrate that eCB2.0 can be used to measure eCB dynamics *in vivo* with high sensitivity and specificity in freely moving animals.

Dual color imaging of eCB and calcium in mouse hippocampal CA1 during running and seizures

Have shown that eCB2.0 enables the detection of electrically evoked eCB signals in mouse hippocampal CA1 in acute slices, we then asked whether we could detect *in vivo* eCB dynamics in CA1 during behavior. We injected AAVs carrying eCB2.0 (or eCBmut) and a red calcium indicator jRGECO1a[67] in mouse CA1, and conducted head-fixed 2P dual-color imaging through an implanted cannula above the hippocampus (**Fig. 6a**). Expression of eCB2.0 and jRGECO1a was clearly observed in CA1 4-6 weeks after virus injection (**Fig. 6b**). We focused on the *stratum pyramidale* layer, which is composed of pyramidal neuron somata and interneuron axons, including a class that densely express CB1R. When mice spontaneously ran on a treadmill (**Fig. 6c**), we found rapid increases of both calcium and eCB signals aligned to the start of running, and decreases of both signals when the running stopped (**Fig. 6d,e**). In the control group, which expressed eCBmut and jRGECO1a, calcium signals were intact while eCBmut showed no fluorescence change (**Fig. 6d,e**). The calcium signal appeared earlier than the eCB signal, although both signals had similar rising kinetics, while the decay phase of eCB signal was slower than that of the calcium signal (**Fig. 6f**). These results demonstrate that under normal physiological conditions, the eCB2.0 sensor enables detection of locomotion-induced eCB signals in mouse hippocampus *in vivo*.

Epilepsy is a neurological disease characterized by excessive and synchronous neuronal firing. eCBs are proposed to provide negative feedback during epilepsy to

attenuate the synaptic activity and protect the nervous system, which is exemplified by the observation that animals with compromised eCB system all exhibit a pro-epileptic phenotype[68]. To explore whether eCB2.0 could be used to study seizure-related eCB signals *in vivo*, we used electrical kindling stimulation of the hippocampus contralateral to the sensor expressing hemisphere to elicit brief self-terminating seizures (**Fig. 6g**). Strong calcium and eCB signal increases were detected during electrical seizure activity (**Fig. 6h**). Recent work has shown that seizures are often followed by a spreading calcium wave that propagates across the cell layer[69]. Interestingly, we also found a propagating eCB wave that closely followed the calcium wave (**Fig. 6h and Extended Data Movie 1**). In contrast, eCBmut showed no response during and after seizures (**Fig. 6i**). The velocity and direction of eCB waves were evident when we extracted the eCB2.0 signal from individual neurons in the field of view (**Fig. 6j,k**). Notably, eCB waves and calcium waves varied across experiment sessions and animals (**Fig. 6l**), but for each instance, the calcium and eCB waves were similar, in agreement with the calcium- and activity-dependence of the eCB signal. In summary, the running and seizure data demonstrate the ability of the eCB2.0 sensor to report eCB dynamics with high specificity and high spatiotemporal resolution in both physiological and pathological conditions *in vivo*.

DISCUSSION

Here, we report the development and characterization of a genetically-encoded fluorescent sensor eCB2.0 for detecting eCBs both *in vitro* and *in vivo*. With high sensitivity, selectivity and kinetics, eCB2.0 enables the detection of endogenous eCB signals in cultured neurons and acute brain slices. eCB2.0 also enables detection of eCB release in the amygdala of freely behaving mice, running induced eCB signals in mouse hippocampus, as well as eCB waves in mouse hippocampus under seizure conditions.

The on kinetics of eCB2.0 measured by local micropressure application at room temperature is ~1.6 s, which is likely overestimated since the on kinetics of eCB2.0 signal in DLS slices and in the BLA *in vivo* was within or about 1 s. The temporal resolution of eCB2.0 is dramatically improved compared to microdialysis (minutes), and it may be further optimized in the future to capture faster signals[70]. Currently, eCB2.0 detects both 2-AG and AEA. Given 2-AG and AEA have different regulatory pathways, brain region and cell type specificities, the development of new sensors with distinct eCB molecular specificity, as well as different color spectra, would be also desirable for future studies.

eCB-mediated retrograde synaptic modulation was identified during the study of depolarization induced suppression of inhibition or excitation (DSI or DSE) in the hippocampus and cerebellum[25,26,28]. Those and subsequent experiments relied on the electrophysiological recordings of synaptic transmission in combination with pharmacological (such as activation and inhibition of cannabinoid receptors, inhibition of production or degradation enzymes) or genetic (such as knockout of corresponding receptors and enzymes) manipulations, thus lacking direct and physiologically relevant eCB detection. Moreover, recording on the somata of neurons is unable to capture the precise spatial distribution of eCBs. For example, DSI recorded from paired whole-cell recordings in hippocampal slices indicate that the depolarization of one neuron could inhibit GABAergic inputs to neurons ~20 μm or less away from it, suggesting the diffusion distance

of eCBs from a single neuron[25]. Similar results were obtained in cerebellar slices using two separate stimulation electrodes to evoke eCB release from two dendritic regions of a single Purkinje cell[56]. These data demonstrate that eCB signaling is relatively local and is likely to be tightly controlled. However, the detailed spatial profile of eCB signal is still not known. In addition, although the sampling rate of electrophysiological recording is generally high (>kHz), the eCB signals revealed by the change of evoked postsynaptic currents (ePSCs) have a sampling interval of ~2 s, which forms a temporal bottleneck. eCB2.0, therefore, for the first time provides the opportunity to examine the eCB signal at high spatial (e.g., synaptic) and temporal (sub-second) resolution, similar to studies using other neurotransmitter sensors[71,72]. In cultured neurons, we detected spontaneous eCB transients with a diameter of ~11 μm, which is already smaller than the previous estimation of the eCB diffusion distance. It will be interesting to test whether the local transient signals originate from single spines.

We have demonstrated that eCB2.0 could be used in multiple preparations *in vitro* and *in vivo* to report real-time neuronal eCB dynamics. Given the complexity of the nervous system, future directions for research based on eCB2.0 applications may include the identity of cell types that release eCBs, the mechanisms and temporal properties of eCB release, characteristics of eCB diffusion, the duration of eCB signals, the nature of the cell types and subcellular elements targeted by eCBs and the effects on them. Answering these fundamental questions will significantly enrich our understanding of the mechanisms and functions of eCB signaling in neural circuits.

Malfunction of eCB system is associated with multiple neurological disorders including stress/anxiety, movement disorders, substance use disorders and epilepsy. The results of eCB detection during foot shock, running and seizure in mice show clear examples of how the eCB2.0 sensor could help to elucidate the fast eCB dynamics during both physiological and pathological processes. The eCB2.0 sensor should be able to detect all CB1R agonists (**Extended Data Fig. 3**) including ∆-9-tetrahydrocannabinol (∆-9-THC) in the brain and periphery following drug administration. This would allow investigators to track the time course of ∆-9-THC actions and the impact of cannabis drugs on eCB signaling. Thus, eCB sensors open a new era of endocannabinoid research aimed at understanding this system at unprecedented, physiologically-relevant spatial and temporal scales.

METHODS

Molecular biology

DNA fragments were amplified by PCR with primers (TSINGKE Biological Technology) containing 25–30 bp overlaps. Plasmids were constructed by restriction enzyme cloning or Gibson Assembly. Plasmid sequences were verified by Sanger sequencing. For characterization of eCB2.0 and eCBmut in HEK293T cells, eCB2.0 and eCBmut genes were cloned into pDisplay vector with a IgK leader sequence before the sensor gene. An IRES-mCherry-CAAX cassette was inserted after the sensor gene for indicating cell membrane and calibrating the sensor fluorescence. For characterization of eCB2.0 in neurons, eCB2.0 gene was cloned into pAAV vector under control of a human synapsin promoter (pAAV-hSyn), PSD95-mScarlet and synaptophysin-mScarlet genes were cloned into pDest vetor under control of a CMV promoter. For the $G_{\beta\gamma}$ sensor assay, human CB1 was cloned into the pCI vector (Promega), eCB2.0 and eCBmut genes were cloned into the peGFP-C1 vector (Takara), replacing the eGFP open reading frame. For the Tango assay, CB1, eCB2.0 and eCBmut genes were cloned into pTango vector. pAAV-hsyn-eCBmut and pAAV-hsyn-R^{ncp}-iGluSnFR were also constructed for virus production.

AAV virus preparation

AAV2/9-hSyn-eCB2.0 ($9.5x10^{13}$ viral genomes (vg)/mL), AAV2/9-hSyn-eCBmut ($8.0x10^{13}$ vg/mL), AAV2/9-hSyn-R^{ncp}-iGluSniFR ($6.2x10^{13}$ vg/mL, all packaged at Vigene Biosciences, China), AAV8-hSyn-mCherry (#114472, Addgene) and AAV1-Syn-NES-jRGECO1a-WPRE-SV40 (Penn Vector Core) were used to infect cultured neurons or *in vivo*.

Cell cultures

HEK293T cells were cultured at 37°C, 5% CO_2 in DMEM (Biological Industries) supplemented with 10% (v/v) fetal bovine serum (Gibco) and penicillin (100 unit/mL)-streptomycin (0.1 mg/mL) (Biological Industries). HEK293T cells were plated on 96-well plates or 12 mm glass coverslips in 24-well plates. Cells at 60–70% confluency were transfected with plasmids using polyethylenimine (PEI) (300 ng DNA/well for 96-well plates and 1 μg DNA/well for 24-well plates, DNA:PEI = 1:3) for 4–6 h before changing fresh culture medium. Imaging was performed 24–36 h after transfection. Rat cortical neurons were prepared from postnatal day 0 (P0) Sprague-Dawley rat. Briefly, rat cortical neurons were dissociated from rat brain cortex after dissection and digestion in 0.25% Trypsin-EDTA (Biological Industries), and plated in 12 mm glass coverslips in 24-well plates coated with poly-D-lysine (Sigma-Aldrich). Neurons were cultured at 37°C, 5% CO_2 in Neurobasal Medium (Gibco) supplemented with 2% B-27 Supplement (Gibco), 1% GlutaMAX (Gibco), and penicillin (100 unit/mL)-streptomycin (0.1 mg/mL) (Biological Industries). Cultured neurons were transfected at 7–9 day *in vitro* (DIV7–9) using calcium phosphate transfection method. Imaging was performed 48 h after transfection. Cultured neurons were infected by AAVs expressing eCB2.0, eCBmut and R^{ncp}-iGluSnFR at DIV3–5, and imaging was performed at DIV12–20. Calbryte590 (AAT Bioquest) was loaded into neurons for 1 h before imaging.

Animals

All experiment protocols were approved by the respective Laboratory Animal Care and Use Committees of Peking University, National Institute on Alcohol Abuse and Alcoholism, Cold Spring Harbor Laboratory (CSHL) and Stanford University, and studies were performed in accordance with the guidelines by the US National Institutes of Health. Postnatal day 0 (P0) Sprague-Dawley rats of both sexes (Beijing Vital River Laboratory) and P42–P150 C57BL/6J mice of both sexes (Beijing Vital River Laboratory and The Jackson Laboratory) were used in this study. Mice were housed under a normal 12 h light/dark cycle with food and water available *ad libitum*.

Confocal imaging in cultured cells

Before imaging, the culture medium for cells was replaced with Tyrode's solution consisting of (in mM): 150 NaCl, 4 KCl, 2 $MgCl_2$, 2 $CaCl_2$, 10 HEPES, and 10 glucose (pH 7.4). 0 mM Ca^{2+} Tyrode's solution contained 0 mM $CaCl^2$ and 2 mM EGTA. The Opera Phenix high-content screening system (PerkinElmer, USA) was used for imaging HEK293T cells in 96-well plates. It was equipped with a 60x/1.15 NA water-immersion objective, a 488 nm laser and a 561 nm laser. A 525/50 nm emission filter and a 600/30 nm emission filter were used to collect green and red fluorescence respectively. A Ti-E A1 confocal microscopy (Nikon, Japan) was used for imaging cultured cells in 12 mm coverslips. It was equipped with a 10x/0.45 NA objective, a 20x/0.75 NA objective, a 40x/1.35 NA oil-immersion objective, a 488 nm laser and a 561 nm laser. A 525/50 nm emission filter and a 595/50 nm emission filter were used to collect green and red fluorescence respectively. Drugs, including 2-AG (Tocris), AEA (Cayman), AM251 (Tocris), LPA (Tocris), S1P (Tocris), ACh (Solarbio), DA (Sigma-Aldrich), GABA (Tocris), Glu (Sigma-Aldrich), Gly, NE (Tocris), 5-HT (Tocris), His (Tocris), Epi (Sigma-Aldrich), Ado (Tocris), Tyr (Sigma-Aldrich), WIN55212-2 (Cayman), DO34 (MCE), JZL184 (Cayman), URB597 (Cayman) were applied by replacing drug-containing Tyrode's solution for 96-well plate imaging, or applied by bath application or by a custom made perfusion system for 12 mm coverslip imaging. The micropressure application of drugs was controlled by Pneumatic PicoPump PV800 (World Precision Instruments). Cultured neurons were field stimulated using parallel platinum electrodes at a distance of 1 cm controlled by a Grass S88 stimulator (Grass Instruments). The voltage was 80 V and the duration of each stimulation pulse was 1 ms.

BRET $G_{\beta\gamma}$ sensor assay

eCB2.0, eCBmut or CB1 genes were transfected using PEI into HEK293 tsA201 cells in 24 well plates in a 1:5 plasmid mass ratio with a single construct designed to separately express human GNAOa, human GNB1 (fused to amino acids 156-239 of Venus), human GNG2 (fused to amino acids 2-155 of Venus) and NanoLuc (Promega) fused to the amino terminal 112 amino acids of human phosducin circularly permutated at amino acids 54/55. The NanoLuc/phosducin fusion portion also contained a kRAS membrane targeting sequence on the carboxy terminal end. The $G_{\beta\gamma}$ sensor components were combined by either restriction enzyme cloning or InFusion (Takara) assembly. Templates for assembly were derived from human whole brain cDNA (Takara) for GNAOa and human retinal cDNA (Takara) for phosducin. Templates for hGNB1 and hGNG2 Venus fusions were a generous

gift from Nevin Lambert (Augusta University). Cells were harvested approximately 24 hours post-transfection with 10mM EDTA in PBS (pH7.2), pelleted and resuspended in Dulbecco's modified PBS (Life Technologies) without calcium or magnesium. Furimazine (Promega) was added at a 1/100 dilution to 100 µl of cell suspension in a black 96 well plate and BRET readings were taken in a Pherastar FS plate reader (Berthold) equipped with a Venus BRET cube. Acceptor (Venus) and donor (NanoLuc) signals were monitored at 535nm and 475nm respectively. Net BRET was calculated as the acceptor/donor ratio of each sample minus the acceptor/donor ratio of a donor only sample. Readings were taken before and 2-4 minutes after agonist 2-AG (Tocris, 20 µM final concentration) application to activate CB1 or eCB sensors.

Tango assay

eCB2.0, eCBmut and CB1R genes fused with the tTA gene in pTango vectors were transfected into the HTLA reporter cell line using the PEI in 6 well plates. The HLTA cell line expresses a β-arrestin2-TEV fusion gene and a tTA-dependent luciferase reporter gene. 24 h after transfection, cells in 6 well plates were collected after trypsin treatment and plated in 96 well plates. CB1R agonist AEA was applied at concentrations ranging from 0.01 nM to 10 µM. The luciferase was expressed for 12 h before the luminescence measurement. Bright-Glo (5 µM, Promega) was added and luminescence was measured by the VICTOR X5 multi-label plate reader (PerkinElmer).

Acute brain slices

Photometry recording in the DLS in acute mouse brain slices

Adult (> 10 weeks) male C57BL/6J mice were anesthetized with isoflurane and injected with AAV vectors into dorsal lateral striatum (300 nL, coordinates relative to bregma in mm: A/P: + 0.75; M/L: ± 2.5; D/V: − 3.5) at a rate of 50 nL/min. Mice were given an injection of ketoprofen (5 mg/kg, s.c.) and postoperative care was provided daily until mice regained their preoperative weight. After a minimum of 4 weeks following AAV injection, mice were deeply anesthetized with isoflurane, decapitated and the brains were extracted and placed in ice cold sucrose cutting solution (in mM): 194 sucrose, 30 NaCl, 4.5 KCl, 26 $NaHCO_3$, 1.2 NaH_2PO_4, 10 D-glucose, 1 $MgCl_2$ saturated with 5% CO_2/ 95% O_2. Coronal brain slices (250 µm) were prepared and slices were incubated at 32°C for ~60 min in artificial cerebrospinal fluid (ACSF) (in mM): 124 NaCl, 4.5 KCl, 26 $NaHCO_3$, 1.2 NaH_2PO_4, 10 D-glucose, 1 $MgCl_2$, 2 $CaCl_2$. After incubation at 32°C, slices were held at room temperature until initiating an experiment. Photometry recordings were acquired using an Olympus BX41 upright epifluorescence microscope equipped with a 40x/0.8 NA water-emersion objective and a FITC filter set. Slices were superfused at ~2 mL/min with ACSF (29–31°C). A twisted bipolar polyimide-coated stainless-steel stimulating electrode (~200 µm tip separation) was placed in the DLS just medial to the corpus callosum and slightly below the tissue surface in a region with visible eCB sensors fluorescence. $GRAB_{eCB}$ sensors were excited using a 470 nm light emitting diode (LED) (ThorLabs, USA). Photons passing through a 180 μm^2 aperture, positioned just lateral to the stimulating electrode, were directed to a PMT (Model D-104, Photon Technology International, USA). The PMT output was amplified (gain: 0.1 µA/V; time constant: 5 ms), filtered at 50 Hz and digitized at 250

Hz using a Digidata 1550B and Clampex software (Molecular Devices LLC, USA). For all experiments, $GRAB_{eCB}$ measurements were acquired as discrete trials repeated every 3 minutes. For each trial, the light exposure period was 35–45 seconds to minimize $GRAB_{eCB}$ photobleaching, while capturing peak responses and the majority of the decay phase. To evoke an eCB transient, a train of electrical pulses (1.0–1.5 mA, 200–500 μs) was delivered 5 s after initiating $GRAB_{eCB}$ excitation.

2-photon imaging in the hippocampus in acute mouse brain slices

Adult (6–8 weeks) C57BL/6J mice of both sexes were anesthetized with an intraperitoneal injection of 2,2,2-tribromoethanol (Avertin, 500 mg/kg body weight, Sigma-Aldrich) and injected with AAV vectors into hippocampal CA1 (400 nL, coordinates relative to bregma in mm: A/P: − 1.8; M/L: ± 1.0; D/V: − 1.2) at a rate of 46 nL/min. After a minimum of 4 weeks following AAV injection, mice were deeply anesthetized with an intraperitoneal injection of 2,2,2-tribromoethanol, decapitated and the brains were extracted and placed in ice cold choline chloride cutting solution (in mM): 110 choline-Cl, 2.5 KCl, 0.5 $CaCl_2$, 7 $MgCl_2$, 1 NaH_2PO_4, 1.3 Na ascorbate, 0.6 Na pyruvate, 25 NaHCO3 and 25 glucose saturated with 5% CO_2/ 95% O_2. Coronal brain slices (300 μm) were prepared and slices were incubated at 34°C for ~40 min in modified ACSF solution (in mM): 125 NaCl, 2.5 KCl, 2 $CaCl_2$, 1.3 $MgCl_2$, 1 NaH_2PO_4, 1.3 Na ascorbate, 0.6 Na pyruvate, 25 $NaHCO_3$ and 25 glucose saturated with 5% CO_2/ 95% O_2. 2-photon imaging were performed under an FV1000MPE 2-photon microscope (Olympus) equipped with a 25x/1.05 NA water-immersion objective and a mode–locked Mai Tai Ti: Sapphire laser (Spectra-Physics). Slices were superfused at ~4 mL/min with modified ACSF (32-34°C). A 920 nm laser was used to excite eCB2.0 sensor, and fluorescence was collected using a 495–540 nm filter. For electrical stimulation, a bipolar electrode (cat. number WE30031.0A3, MicroProbes for Life Science) was positioned near the Stratum radiatum layer in CA1 using fluorescence guidance. Fluorescence imaging and electrical stimulation were synchronized using an Arduino board with custom-written programs. All images collected during electrical stimulation were recorded at a frame rate of 0.3583 s/frame with 256×192 pixels per frame. The stimulation voltage was 4–6 V, and the pulse duration was 1 ms. Drugs were applied to the imaging chamber by perfusion at a flow rate at 4 mL/min.

Fiber photometry recording of eCB signals in the BLA during foot shock

Adult (10–12 weeks) C57 BL/6J mice of both sexes were injected with 300 nL of a 10:1 mixture of AAV-hSyn-eCB2.0 and AAV-hSyn-mCherry viruses, or a 10:1 mixture of AAV-hSyn-eCBmut and AAV-hSyn-mCherry viruses, into the right basolateral amygdala at A/P −1.78 mm, M/L −3.30 mm, D/V −4.53 mm (relative to Bregma). Virus injection was performed using a glass pipette with a Picospritzer III microinjection system (Parker Hannifin, USA). After injection, a 200-μm-diameter, 0.37 NA fiber (Inper, China) was implanted into the same location, and secured with self-adhesive resin cement (3M). A head bar was also mounted with resin cement onto the skull. At least 14 days were waited before doing photometry recording. Photometry recording was taken using a commercial photometry system (Neurophotometrics, USA). A patch cord (0.37 NA, Doric Lenses, Canada) was attached to the photometry system, and to the fiber in the mouse brain. A 470 nm LED was used to excite eCB and eCBmut sensors, and a 560 nm LED was used

to excite mCherry. The average power levels of LED (measured at the output end of the patch cord) were 160 µW for eCB/eCBmut sensors, and 25 µW for mCherry. The recording frequency was 10 Hz. Photometry data were acquired with Bonsai 2.3.1 software. Mice were free-moving in a shock box (Habitest, Coulbourn Instruments, USA) inside of a sound-proof behavior box with light on. The FreezeFrame software was used to generate triggers to the shock generator (Coulbourn Instruments) and Bonsai software. Five pulses of 2-s electric shocks with an intensity of 0.7 mA were delivered to the shock box with 90–120 s ITIs. After photometry recording, animals were perfused with phosphate-buffered saline (PBS), and subsequently with 4% paraformaldehyde (PFA) in PBS. Brain tissues were fixed in PFA solution overnight, and then were dehydrated with 30% sucrose in PBS solution for 24 h. Brain slices were cut using a Leica SM 2010R microtome (Leica Biosystems, USA). Floating brain slices were blocked (5% BSA, 0.1% Triton in PBS) at room temperature for 2 h, and then stained with chicken anti-GFP (1:1000, Aves, #GFP-1020) and rabbit anti-RFP (1:500, Rockland, #600-401-379) primary antibodies in antibody solution (3% BSA, 0.1% Triton in PBS) at 4 °C for 24 h. Slices were next rinsed with PBS 15 min for 3 times, and stained with DAPI (5 µg/mL, Invitrogen, #D1306), Alexa Fluor 488 donkey anti-chicken (1:250, Jackson ImmunoResearch, #703-545-155) and Alexa Fluor 568 donkey anti-rabbit (1:250, Invitrogen, #A10042) in antibody solution at 4 °C for 24 h. Confocal images were taken with a Zeiss LSM780 confocal microscopy (Zeiss, Germany).

2-photon imaging in living mice

Adult (P100− 150) C57BL/6J mice of both sexes were used. Mice were injected with a mix of AAV1-Syn-NES-jRGECO1a-WPRE-SV40 and AAV9-hSyn-eCB2.0 (or eCBmut) viruses (300-400 nL each, full titer) into the right CA1 (2.3 mm posterior, 1.5 mm lateral, 1.35 mm ventral to bregma) using a Hamilton syringe. After recovery from virus injection, the cortex above the injection site was aspirated and a stainless steel cannula with attached coverglass was implanted over the hippocampus as previously described[73,74], followed by a stainless steel headbar. A chronic bipolar wire electrode (tungsten, 0.002”, 0.5 mm tip separation, A-M systems) was implanted into the left ventral hippocampus (3.2 mm posterior, 2.7 mm lateral, 4.0 mm ventral to bregma) as previously described[75]. Head-fixed mice running on a linear treadmill with a cue-less belt (2 m) were imaged using a resonant scanner 2-photon microscope (Neurolabware), equipped with a pulsed IR laser tuned at 1000 nm (Mai Tai, Spectra-Physics), GaAsP PMT detectors (H11706P-40, Hamamatsu), and a 16x objective (0.8 NA WI, Nikon). 2-photon image acquisition and treadmill speed monitoring were controlled by Scanbox (Neurolabware). Bipolar electrodes were recorded using a differential amplifier (Model 1700, A-M Systems). Seizures were elicited by electric stimulation above seizure threshold by 150 µA of current delivered in 1ms biphasic pulses at 60Hz for 1 second, using a constant-current stimulator (A-M Systems model 2100). Following *in vivo* recordings, mice were anaesthetized by isoflurane, prior to an intraperitoneal injection of a mixture of ketamine (100 mg/kg) and Xylazine (10 mg/kg) in saline. Animals were transcardially perfused with saline (0.9% NaCl for 1 minute) and then with fixative solution (4% paraformaldehyde and 0.2% picric acid in 0.1 M phosphate buffer). Perfused brains were then post-fixed in the same fixative solution for 24 h at 4 °C, prior to slicing on a vibratome (VTS1200, Leica Biosystems). Sections were then washed and

mounted in Vectashield (Vector Laboratories). Confocal images were acquired on a Zeiss LSM 710 imaging system using a 20x 0.8 NA objective.

Data processing

Confocal imaging

Data were collected and analyzed using Harmony high-content imaging and analysis software (PerkinElmer) for 96-well plate imaging. Briefly, membrane regions were selected as ROIs and green fluorescence of sensors was normalized by red fluorescence of mCherry-CAAX (G/R). $\Delta F/F_0$ was calculated as $(G/R_{after\ durg} - G/R_{before\ drug}) / (G/R_{before\ drug})$. For 12 mm coverslip imaging, data were collected using the NIS-Element software (Nikon) and analyzed using the ImageJ software (NIH). $\Delta F/F_0$ was calculated as $(F_t - F_0)/F_0$, while F_0 was quantified before drug application or stimulation. Data were plotted using OriginPro 2020 (OriginLab).

Slice photometry and 2-photon imaging

For slice photometry recording, eCB transients were calculated as $\Delta F/F_0$ by averaging the PMT voltage (V) for a period of 1 s just prior to electrical stimulation (F_0) and then calculating V/F_0-1 for each digitized data sample. The eCB decay phase was fitted with a single exponential decay accounting for a sloping baseline. Rise $t_{1/2}$ was calculated in Graphpad Prism (v8.3; San Diego, CA, USA) by fitting the rising phase of the eCB transient with an asymmetrical logistics curve. Photometry sweeps were exported to Microsoft Excel (v16.3; Redmond, WA, USA) to calculate normalized $\Delta F/F_0$ traces and peak $\Delta F/F_0$ values. For slice 2-photon imaging, data were collected using FV10-ASW (Olympus) and analyzed using ImageJ (NIH). $\Delta F/F_0$ was calculated as $(F_t - F_0)/F_0$, while F_0 was quantified before stimulation. Data were plotted using OriginPro 2020 (OriginLab).

Fiber photometry in mice during foot shock

Off-line analysis of the photometry data was conducted with the Matlab software (MathWorks). Data were plotted using OriginPro 2020 (OriginLab).

2-photon imaging in mice during locomotion and seizure

Imaging data were processed and analyzed using Python scripts. For the analysis of single-cell responses, movies were initially motion corrected by rigid translation, followed by non-rigid correction (*HiddenMarkov2D*) by the sima package[76]. Binary regions of interest (ROIs) were selected in a semi-automated manner. For the initial automated detection, movies were divided into segments of 100 frames each, the average intensity projection of each segment was computed and the resulting resampled movie was used for detection. In sessions with electric stimulation, only the baseline period before the stimulation was used for segmentation. The *PlaneCA1PC* method of sima was run on the inverted resampled movie, which resulted in detection of the hollow nuclei of cells. These ROIs were filtered based on size, and binary dilation was performed to include the cytoplasm around the nuclei. In a subsequent step, ROIs were detected in the non-inverted resampled movie, filtered based on size and those that did not overlap with existing ROIs were added to the set. ROIs outside the str. pyramidale were excluded. Next, the fluorescence intensity traces were extracted for each ROI by averaging the included pixel intensities within each frame. For analyzing run responses, only sessions with no electric stimuli were included, and signals were pulled from the motion-corrected movies. These

raw traces were processed following standard steps for obtaining $\Delta F/F_0$ traces with a modified approach to determine the time-dependent baseline. A 3rd degree polynomial was fit on the trace after applying temporal smoothing, removing peaks (detected using continuous wavelet transform by scipy.signal), eliminating periods of running, and ignoring the beginning and end of the recording. The calculated polynomial was then used as a baseline. Z-scored traces were obtained after determining the standard deviation (SD) of each cell's baseline by excluding events exceeding 2 SD in two iterations.

For analyzing spreading activity, only sessions with electric stimulus that triggered an electrographic seizure and a spreading wave were included, and while the segmentation was performed based on the motion-corrected baseline segments of the recordings, signals were pulled from non-motion-corrected movies (as image-based motion correction was not feasible during seizures). $\Delta F/F_0$ traces were obtained using a constant baseline determined by averaging the pre-stimulus segments of the traces. For the analysis changes in average fluorescence intensity, a single large region of interest (ROI) was manually drawn to include the cell bodies in the pyramidal layer, and $\Delta F/F_0$ traces were pulled and processed as described above. Event-triggered averages were calculated after automatically detecting the frames with running onsets and stops by fixed criteria across all sessions. The average was computed in two steps (i.e. events were first averaged by cell, then cells averaged by virus type (eCB or eCBmut). Decay time constants were computed as the parameter of a 2nd degree polynomial fit after a log transform on the trace following the peak of the stop-triggered average trace. Rise times were determined between the frame where the start-triggered average signal first reached 90% of the range between baseline and peak, and the last frame before that where the signal was below 10% of the range. To determine the spreading speed and direction of waves, first the peak time of the wave was determined in each session by inspecting the average $\Delta F/F_0$ trace (including all cells). Then, the relative peak location (Δt) of the $\Delta F/F_0$ trace of each cell in the trace including ± 200 frames (12.8 s) around the wave peak was determined. Finally, two linear fits were computed using the x and y centroid coordinates of each ROI ($\Delta t \sim x$, $\Delta t \sim y$). The 2D speed was computed from the slopes of the two 1D fits. The direction was determined by computing the unity vector from the starting- to the end point of the fits between ± 3 s around the wave peak. The average speed was obtained by averaging the speed of individual sessions, while the average direction was obtained from the sum of the unity vectors of individual sessions. Data were plotted using Python and OriginPro 2020 (OriginLab).

Statistical analysis

Values with error bars indicate mean ± SEM. Group data were analyzed using the Student's t test or one-way ANOVA, ***$p < 0.001$, **$p < 0.01$, *$p < 0.05$; n.s., not significant, $p > 0.05$.

Data and software availability

Plasmids for expressing eCB2.0 and eCBmut used in this study were deposited at Addgene (https://www.addgene.org/Yulong_Li/).

ACKNOWLEDGMENTS

This work was supported by Beijing Municipal Science & Technology Commission (Z181100001318002, Z181100001518004), National Natural Science Foundation of China (31925017), NIH BRAIN Initiative (NS103558), Shenzhen-Hong Kong Institute of Brain Science (NYKFKT2019013) and grants from the Peking-Tsinghua Center for Life Sciences and the State Key Laboratory of Membrane Biology at Peking University School of Life Sciences to Y.L.; a Division of Intramural Clinical and Biological Research of the NIAAA grant (ZIA AA000416) to D.M.L; a NIH BRAIN Initiative (NS103558) grant to J.D.; NIH grants (R01MH101214 and R01NS104944) to B.L.; an American Epilepsy Society Postdoctoral Fellowship and a NIH grant (K99NS117795) to B.D.; a Canadian Institutes for Health Research postdoctoral fellowship to J.S.F.; a NIH grant to I.S. (NS99457). We thank Li lab members for helpful discussions. We thank Yi Rao for sharing the 2-photon microscope and Xiaoguang Lei at PKU-CLS for providing support for the Opera Phenix high-content screening system.

AUTHOR CONTRIBUTIONS

Y.L. conceived the project. A.D., K.H., H.L.P., R.C. and J.D. performed experiments related to developing, optimizing, and characterizing the sensors in cultured HEK293T cells and neurons. L.J.D. performed the surgery and photometry recording experiments related to the validation of the sensor in DLS brain slices under the supervision of D.M.L.. A.D. performed the surgery and 2-photon imaging in the hippocampal brain slices. E.A. performed the surgery and 2-photon imaging in the striatal brain slices under the supervision of J.D.. W. G. performed fiber photometry recordings in freely moving mice during foot shock under the supervision of B.L.. B.D. and J.S.F. performed the *in vivo* 2-photon imaging in the hippocampus in mice during running and seizure under the supervision of I.S. All authors contributed to the data interpretation and analysis. A.D. and Y.L. wrote the manuscript with input from other authors.

COMPETING FINANCIAL INTERESTS

Y. L. has filed patent applications whose value might be affected by this publication.

REFERENCES

1. Zuardi, A.W. History of cannabis as a medicine: a review. *Braz J Psychiatry* **28**, 153-157 (2006).
2. Piomelli, D. The molecular logic of endocannabinoid signalling. *Nat Rev Neurosci* **4**, 873-884 (2003).
3. Wilson, R.I. & Nicoll, R.A. Endocannabinoid signaling in the brain. *Science* **296**, 678-682 (2002).
4. Kano, M., Ohno-Shosaku, T., Hashimotodani, Y., Uchigashima, M. & Watanabe, M. Endocannabinoid-mediated control of synaptic transmission. *Physiological reviews* **89**, 309-380 (2009).
5. Hebert-Chatelain, E.*, et al.* A cannabinoid link between mitochondria and memory. *Nature* **539**, 555-559 (2016).
6. Benard, G.*, et al.* Mitochondrial CB(1) receptors regulate neuronal energy metabolism. *Nat*

693 *Neurosci* **15**, 558-564 (2012).
694 7. Jimenez-Blasco, D.*, et al.* Glucose metabolism links astroglial mitochondria to cannabinoid
695 effects. *Nature* **583**, 603-608 (2020).
696 8. Stella, N. Cannabinoid signaling in glial cells. *Glia* **48**, 267-277 (2004).
697 9. Navarrete, M., Diez, A. & Araque, A. Astrocytes in endocannabinoid signalling. *Philos*
698 *Trans R Soc Lond B Biol Sci* **369**, 20130599 (2014).
699 10. Chevaleyre, V., Takahashi, K.A. & Castillo, P.E. Endocannabinoid-mediated synaptic
700 plasticity in the CNS. *Annu Rev Neurosci* **29**, 37-76 (2006).
701 11. Oddi, S., Scipioni, L. & Maccarrone, M. Endocannabinoid system and adult neurogenesis:
702 a focused review. *Curr Opin Pharmacol* **50**, 25-32 (2020).
703 12. Moreira, F.A. & Lutz, B. The endocannabinoid system: emotion, learning and addiction.
704 *Addict Biol* **13**, 196-212 (2008).
705 13. Guindon, J. & Hohmann, A.G. The endocannabinoid system and pain. *CNS Neurol Disord*
706 *Drug Targets* **8**, 403-421 (2009).
707 14. Kesner, A.J. & Lovinger, D.M. Cannabinoids, Endocannabinoids and Sleep. *Frontiers in*
708 *molecular neuroscience* **13**, 125 (2020).
709 15. Silvestri, C. & Di Marzo, V. The endocannabinoid system in energy homeostasis and the
710 etiopathology of metabolic disorders. *Cell Metab* **17**, 475-490 (2013).
711 16. Katona, I. & Freund, T.F. Endocannabinoid signaling as a synaptic circuit breaker in
712 neurological disease. *Nat Med* **14**, 923-930 (2008).
713 17. Fernandez-Espejo, E., Viveros, M.P., Nunez, L., Ellenbroek, B.A. & Rodriguez de Fonseca,
714 F. Role of cannabis and endocannabinoids in the genesis of schizophrenia.
715 *Psychopharmacology (Berl)* **206**, 531-549 (2009).
716 18. Fraguas-Sanchez, A.I., Martin-Sabroso, C. & Torres-Suarez, A.I. Insights into the effects
717 of the endocannabinoid system in cancer: a review. *Br J Pharmacol* **175**, 2566-2580 (2018).
718 19. Patel, S., Hill, M.N., Cheer, J.F., Wotjak, C.T. & Holmes, A. The endocannabinoid system
719 as a target for novel anxiolytic drugs. *Neurosci Biobehav Rev* **76**, 56-66 (2017).
720 20. Ligresti, A., Petrosino, S. & Di Marzo, V. From endocannabinoid profiling to
721 'endocannabinoid therapeutics'. *Curr Opin Chem Biol* **13**, 321-331 (2009).
722 21. Sabatini, B.L. & Regehr, W.G. Timing of synaptic transmission. *Annu Rev Physiol* **61**, 521-
723 542 (1999).
724 22. van den Pol, A.N. Neuropeptide transmission in brain circuits. *Neuron* **76**, 98-115 (2012).
725 23. Zoerner, A.A.*, et al.* Quantification of endocannabinoids in biological systems by
726 chromatography and mass spectrometry: a comprehensive review from an analytical and
727 biological perspective. *Biochim Biophys Acta* **1811**, 706-723 (2011).
728 24. Marchioni, C.*, et al.* Recent advances in LC-MS/MS methods to determine
729 endocannabinoids in biological samples: Application in neurodegenerative diseases. *Anal Chim*
730 *Acta* **1044**, 12-28 (2018).
731 25. Wilson, R.I. & Nicoll, R.A. Endogenous cannabinoids mediate retrograde signalling at
732 hippocampal synapses. *Nature* **410**, 588-592 (2001).
733 26. Kreitzer, A.C. & Regehr, W.G. Retrograde inhibition of presynaptic calcium influx by
734 endogenous cannabinoids at excitatory synapses onto Purkinje cells. *Neuron* **29**, 717-727
735 (2001).
736 27. Maejima, T., Hashimoto, K., Yoshida, T., Aiba, A. & Kano, M. Presynaptic inhibition caused

737 by retrograde signal from metabotropic glutamate to cannabinoid receptors. *Neuron* **31**, 463-
738 475 (2001).
739 28. Ohno-Shosaku, T., Maejima, T. & Kano, M. Endogenous cannabinoids mediate retrograde
740 signals from depolarized postsynaptic neurons to presynaptic terminals. *Neuron* **29**, 729-738
741 (2001).
742 29. Wiskerke, J.*, et al.* Characterization of the effects of reuptake and hydrolysis inhibition on
743 interstitial endocannabinoid levels in the brain: an in vivo microdialysis study. *ACS Chem*
744 *Neurosci* **3**, 407-417 (2012).
745 30. Walker, J.M., Huang, S.M., Strangman, N.M., Tsou, K. & Sanudo-Pena, M.C. Pain
746 modulation by release of the endogenous cannabinoid anandamide. *Proc Natl Acad Sci U S A*
747 **96**, 12198-12203 (1999).
748 31. Sun, F.*, et al.* A Genetically Encoded Fluorescent Sensor Enables Rapid and Specific
749 Detection of Dopamine in Flies, Fish, and Mice. *Cell* **174**, 481-496 e419 (2018).
750 32. Patriarchi, T.*, et al.* Ultrafast neuronal imaging of dopamine dynamics with designed
751 genetically encoded sensors. *Science* **360**(2018).
752 33. Jing, M.*, et al.* A genetically encoded fluorescent acetylcholine indicator for in vitro and in
753 vivo studies. *Nat Biotechnol* **36**, 726-737 (2018).
754 34. Feng, J.*, et al.* A Genetically Encoded Fluorescent Sensor for Rapid and Specific In Vivo
755 Detection of Norepinephrine. *Neuron* **102**, 745-761 e748 (2019).
756 35. Peng, W.*, et al.* Regulation of sleep homeostasis mediator adenosine by basal forebrain
757 glutamatergic neurons. *Science* **369**(2020).
758 36. Patriarchi, T.*, et al.* An expanded palette of dopamine sensors for multiplex imaging in vivo.
759 *Nat Methods* (2020).
760 37. Jing, M.*, et al.* An optimized acetylcholine sensor for monitoring in vivo cholinergic activity.
761 *Nature Methods* (2020).
762 38. Sun, F.*, et al.* New and improved GRAB fluorescent sensors for monitoring dopaminergic
763 activity in vivo. 2020.2003.2028.013722 (2020).
764 39. Wan, J.*, et al.* A genetically encoded GRAB sensor for measuring serotonin dynamics
765 in vivo. 2020.2002.2024.962282 (2020).
766 40. Howlett, A.C.*, et al.* International Union of Pharmacology. XXVII. Classification of
767 cannabinoid receptors. *Pharmacol Rev* **54**, 161-202 (2002).
768 41. Hua, T.*, et al.* Crystal structures of agonist-bound human cannabinoid receptor CB1.
769 *Nature* **547**, 468-471 (2017).
770 42. Hua, T.*, et al.* Crystal Structure of the Human Cannabinoid Receptor CB1. *Cell* **167**, 750-
771 762 e714 (2016).
772 43. Krishna Kumar, K.*, et al.* Structure of a Signaling Cannabinoid Receptor 1-G Protein
773 Complex. *Cell* **176**, 448-458 e412 (2019).
774 44. Li, X.*, et al.* Crystal Structure of the Human Cannabinoid Receptor CB2. *Cell* **176**, 459-467
775 e413 (2019).
776 45. Shao, Z.*, et al.* Structure of an allosteric modulator bound to the CB1 cannabinoid receptor.
777 *Nat Chem Biol* **15**, 1199-1205 (2019).
778 46. Shao, Z.*, et al.* High-resolution crystal structure of the human CB1 cannabinoid receptor.
779 *Nature* (2016).
780 47. Masuho, I.*, et al.* Distinct profiles of functional discrimination among G proteins determine

781 the actions of G protein-coupled receptors. *Sci Signal* **8**, ra123 (2015).
782 48. Hollins, B., Kuravi, S., Digby, G.J. & Lambert, N.A. The c-terminus of GRK3 indicates rapid
783 dissociation of G protein heterotrimers. *Cell Signal* **21**, 1015-1021 (2009).
784 49. Kroeze, W.K.*, et al.* PRESTO-Tango as an open-source resource for interrogation of the
785 druggable human GPCRome. *Nat Struct Mol Biol* **22**, 362-369 (2015).
786 50. Kim, S.H., Won, S.J., Mao, X.O., Jin, K. & Greenberg, D.A. Molecular mechanisms of
787 cannabinoid protection from neuronal excitotoxicity. *Mol Pharmacol* **69**, 691-696 (2006).
788 51. Wu, J.*, et al.* Genetically Encoded Glutamate Indicators with Altered Color and Topology.
789 *ACS Chem Biol* **13**, 1832-1837 (2018).
790 52. Alger, B.E. Retrograde signaling in the regulation of synaptic transmission: focus on
791 endocannabinoids. *Prog Neurobiol* **68**, 247-286 (2002).
792 53. Ogasawara, D.*, et al.* Rapid and profound rewiring of brain lipid signaling networks by
793 acute diacylglycerol lipase inhibition. *Proc Natl Acad Sci U S A* **113**, 26-33 (2016).
794 54. Long, J.Z.*, et al.* Selective blockade of 2-arachidonoylglycerol hydrolysis produces
795 cannabinoid behavioral effects. *Nat Chem Biol* **5**, 37-44 (2009).
796 55. Mor, M.*, et al.* Cyclohexylcarbamic acid 3'- or 4'-substituted biphenyl-3-yl esters as fatty
797 acid amide hydrolase inhibitors: synthesis, quantitative structure-activity relationships, and
798 molecular modeling studies. *J Med Chem* **47**, 4998-5008 (2004).
799 56. Brenowitz, S.D. & Regehr, W.G. Associative short-term synaptic plasticity mediated by
800 endocannabinoids. *Neuron* **45**, 419-431 (2005).
801 57. Soler-Llavina, G.J. & Sabatini, B.L. Synapse-specific plasticity and compartmentalized
802 signaling in cerebellar stellate cells. *Nat Neurosci* **9**, 798-806 (2006).
803 58. Lerner, T.N. & Kreitzer, A.C. RGS4 is required for dopaminergic control of striatal LTD and
804 susceptibility to parkinsonian motor deficits. *Neuron* **73**, 347-359 (2012).
805 59. Gerdeman, G.L., Ronesi, J. & Lovinger, D.M. Postsynaptic endocannabinoid release is
806 critical to long-term depression in the striatum. *Nat Neurosci* **5**, 446-451 (2002).
807 60. Kreitzer, A.C. & Malenka, R.C. Endocannabinoid-mediated rescue of striatal LTD and
808 motor deficits in Parkinson's disease models. *Nature* **445**, 643-647 (2007).
809 61. Yasuda, H., Huang, Y. & Tsumoto, T. Regulation of excitability and plasticity by
810 endocannabinoids and PKA in developing hippocampus. *Proc Natl Acad Sci U S A* **105**, 3106-
811 3111 (2008).
812 62. Edwards, D.A., Zhang, L. & Alger, B.E. Metaplastic control of the endocannabinoid system
813 at inhibitory synapses in hippocampus. *Proc Natl Acad Sci U S A* **105**, 8142-8147 (2008).
814 63. Li, B. Central amygdala cells for learning and expressing aversive emotional memories.
815 *Curr Opin Behav Sci* **26**, 40-45 (2019).
816 64. Katona, I.*, et al.* Distribution of CB1 cannabinoid receptors in the amygdala and their role
817 in the control of GABAergic transmission. *J Neurosci* **21**, 9506-9518 (2001).
818 65. Morena, M., Patel, S., Bains, J.S. & Hill, M.N. Neurobiological Interactions Between Stress
819 and the Endocannabinoid System. *Neuropsychopharmacology* **41**, 80-102 (2016).
820 66. Gunduz-Cinar, O., Hill, M.N., McEwen, B.S. & Holmes, A. Amygdala FAAH and
821 anandamide: mediating protection and recovery from stress. *Trends Pharmacol Sci* **34**, 637-
822 644 (2013).
823 67. Dana, H.*, et al.* Sensitive red protein calcium indicators for imaging neural activity. *Elife*
824 **5**(2016).

825 68. Soltesz, I.*, et al.* Weeding out bad waves: towards selective cannabinoid circuit control in
826 epilepsy. *Nat Rev Neurosci* **16**, 264-277 (2015).
827 69. Farrell, J.S.*, et al.* In vivo assessment of mechanisms underlying the neurovascular basis
828 of postictal amnesia. *Sci Rep* **10**, 14992 (2020).
829 70. Heinbockel, T.*, et al.* Endocannabinoid signaling dynamics probed with optical tools. *J*
830 *Neurosci* **25**, 9449-9459 (2005).
831 71. Ju, N.*, et al.* Spatiotemporal functional organization of excitatory synaptic inputs onto
832 macaque V1 neurons. *Nat Commun* **11**, 697 (2020).
833 72. Sethuramanujam, S.*, et al.* Rapid 'multi-directed' cholinergic transmission at central
834 synapses. 2020.2004.2018.048330 (2020).
835 73. Kaifosh, P., Lovett-Barron, M., Turi, G.F., Reardon, T.R. & Losonczy, A. Septo-hippocampal
836 GABAergic signaling across multiple modalities in awake mice. *Nat Neurosci* **16**, 1182-1184
837 (2013).
838 74. Lovett-Barron, M.*, et al.* Dendritic inhibition in the hippocampus supports fear learning.
839 *Science* **343**, 857-863 (2014).
840 75. Farrell, J.S.*, et al.* Postictal behavioural impairments are due to a severe prolonged
841 hypoperfusion/hypoxia event that is COX-2 dependent. *Elife* **5**(2016).
842 76. Kaifosh, P., Zaremba, J.D., Danielson, N.B. & Losonczy, A. SIMA: Python software for
843 analysis of dynamic fluorescence imaging data. *Front Neuroinform* **8**, 80 (2014).
844

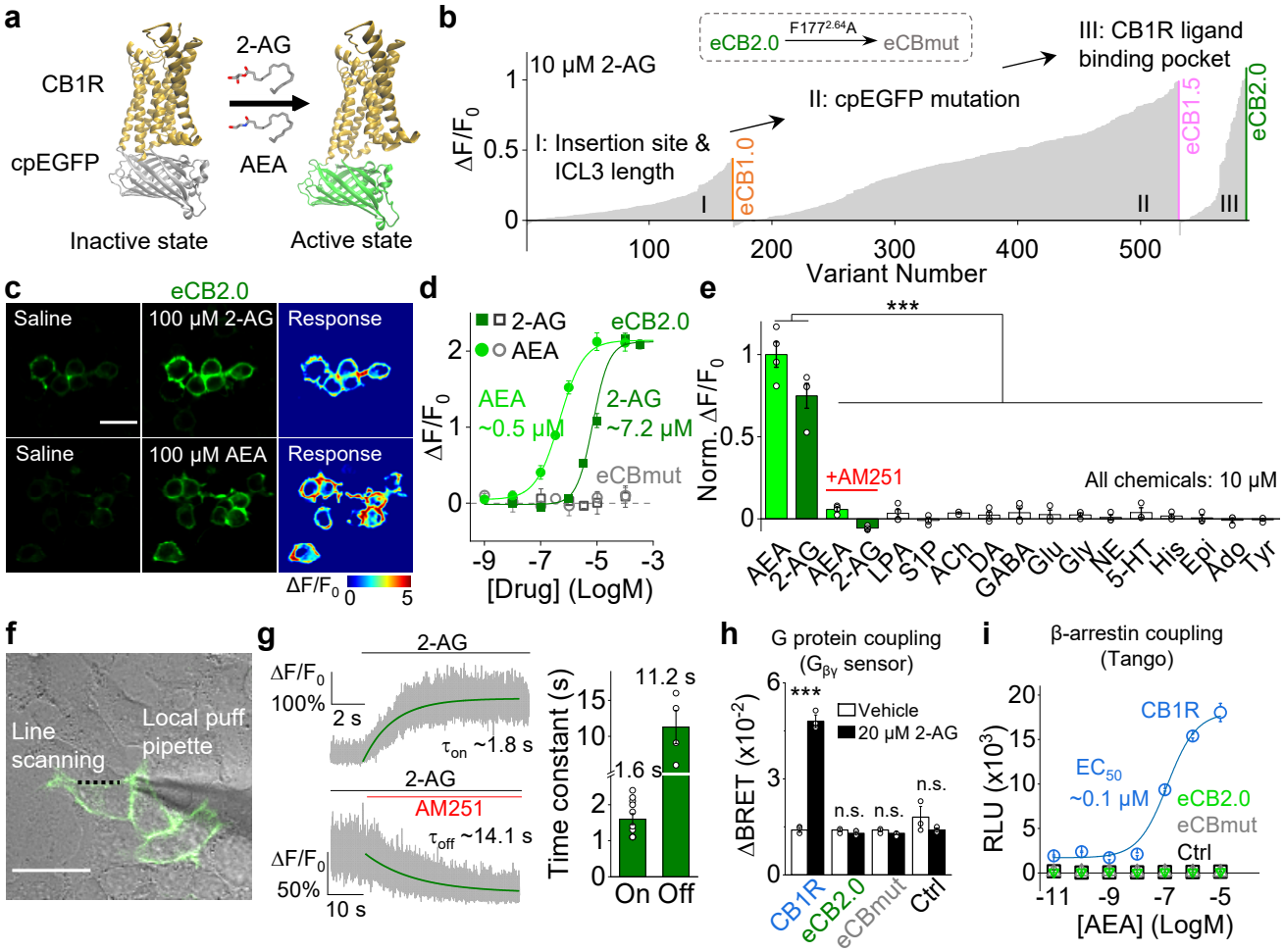

Fig. 1 | Development and characterization of GRAB$_{eCB}$ sensors in HEK293T cells

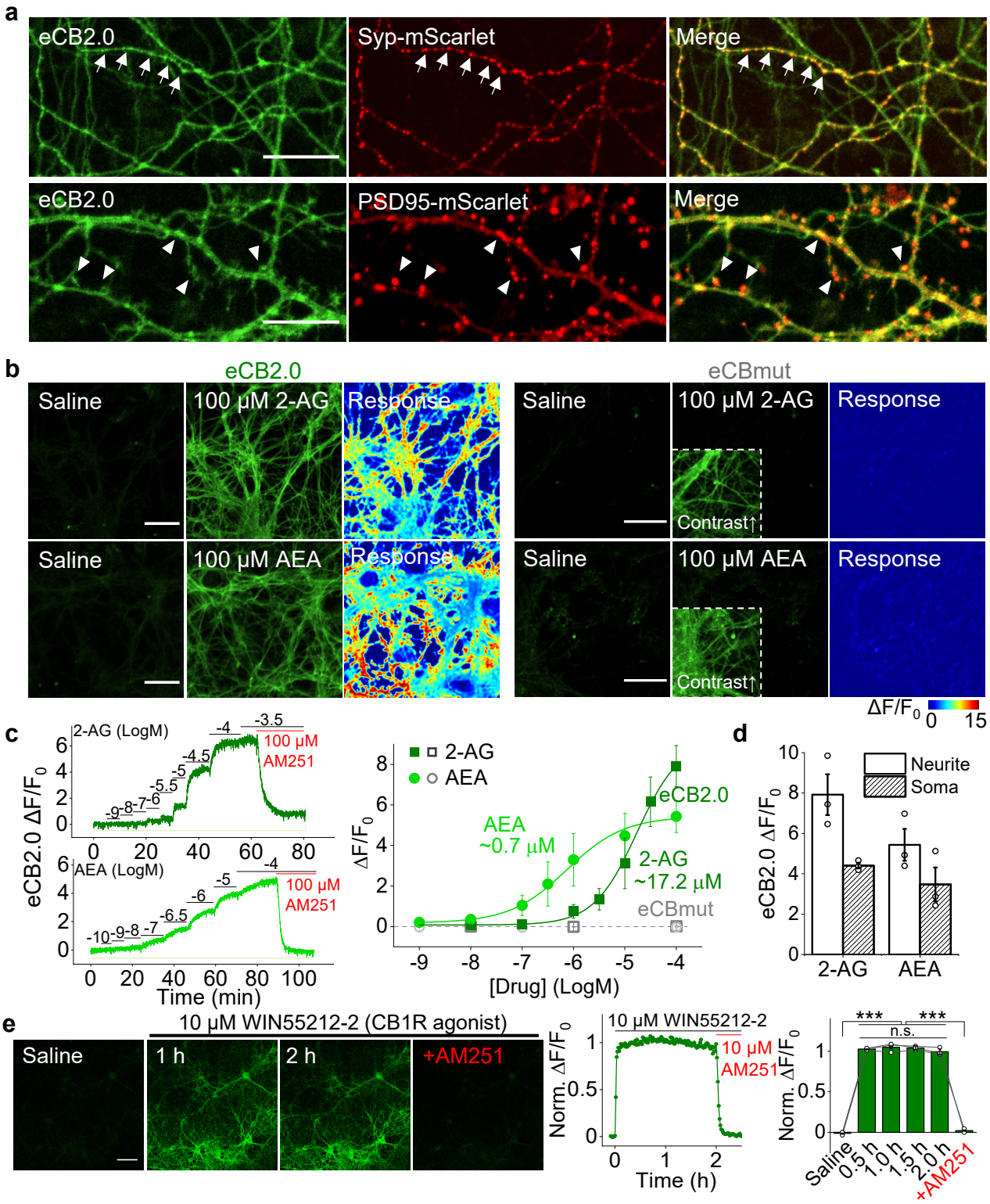

Fig. 2 | Characterization of GRAB$_{eCB}$ in primary cultured neurons

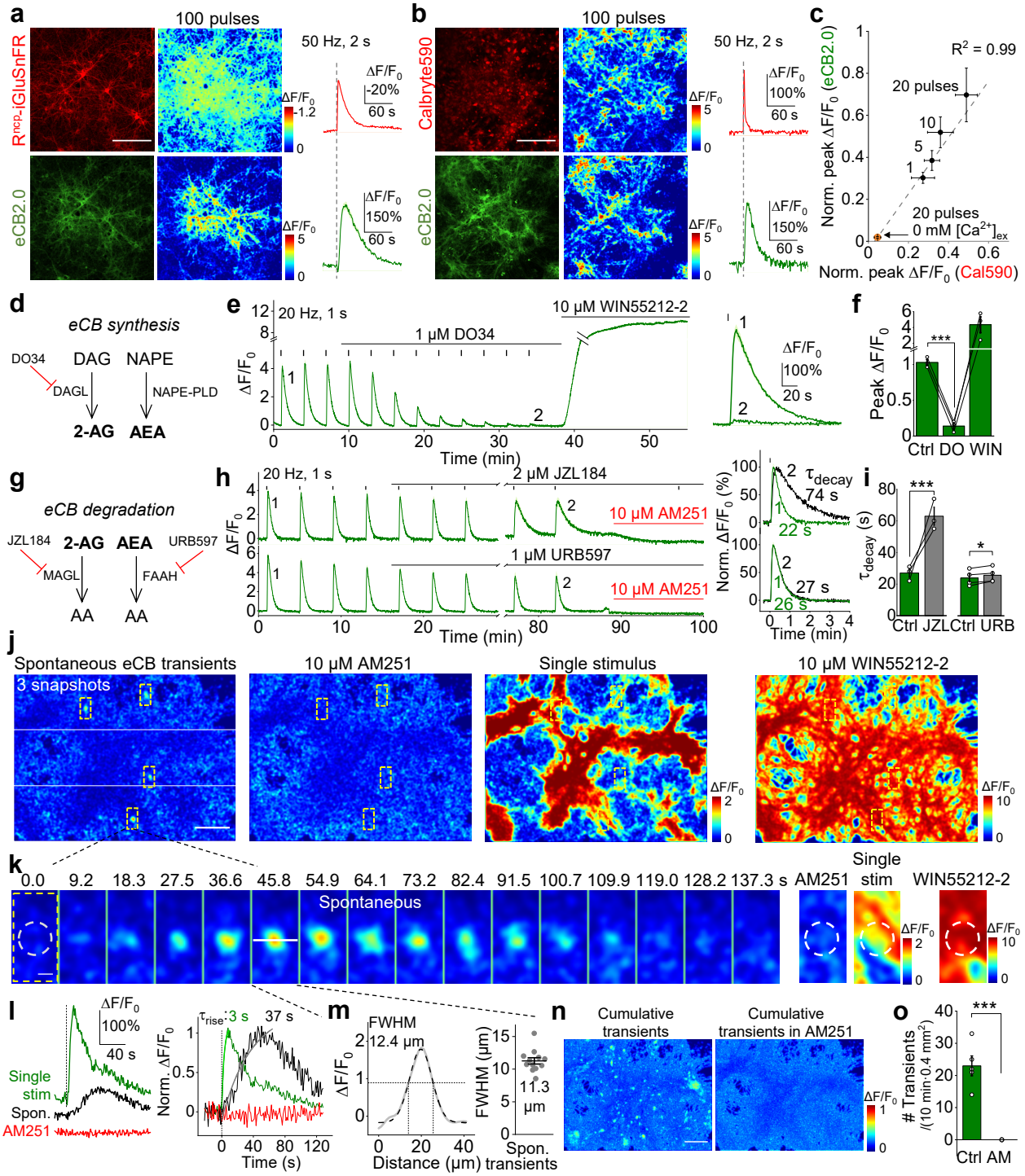

Fig. 3 | Imaging endogenously released eCBs in primary cultured neurons

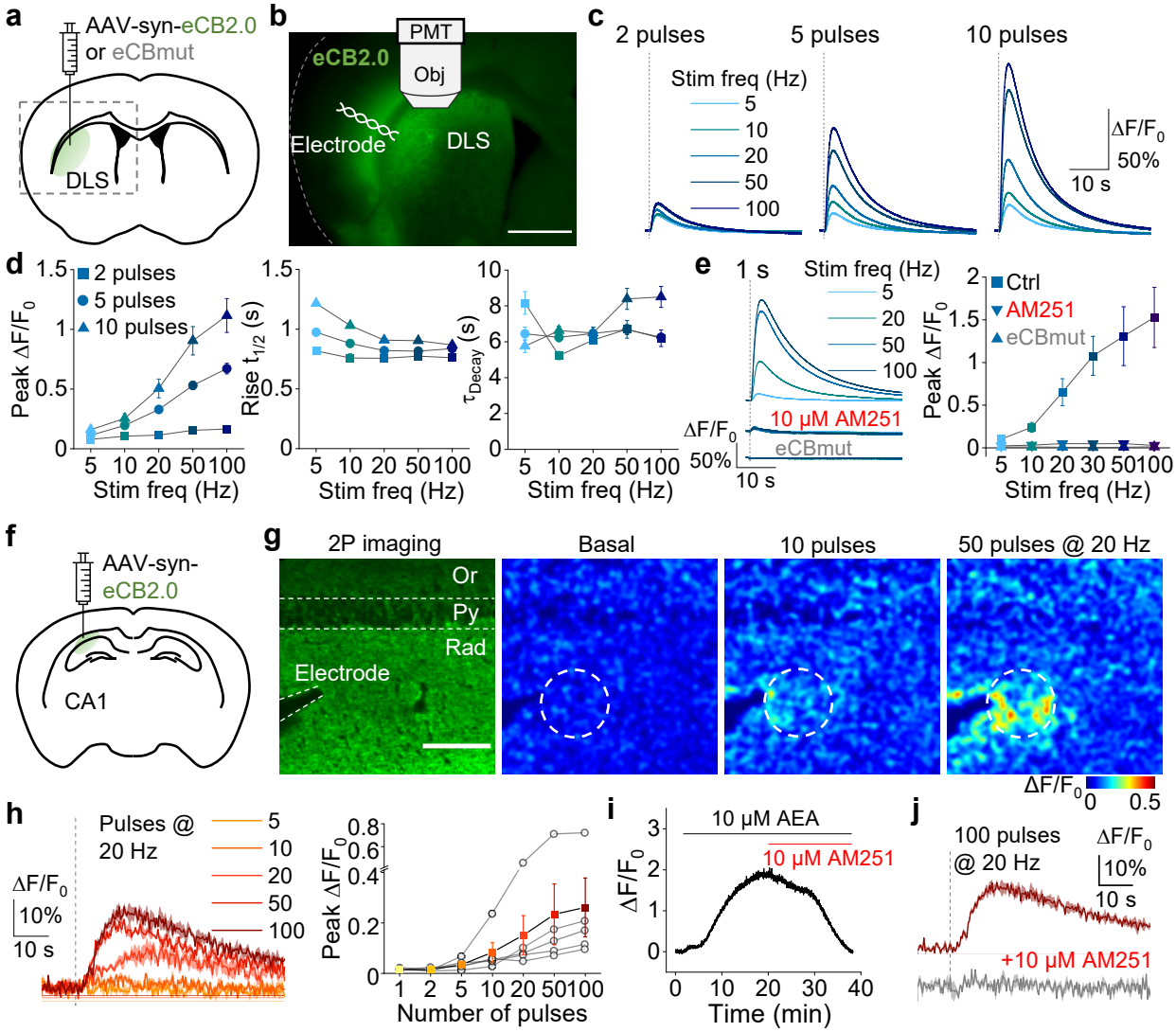

Fig. 4 | Detection of eCBs in acute brain slices

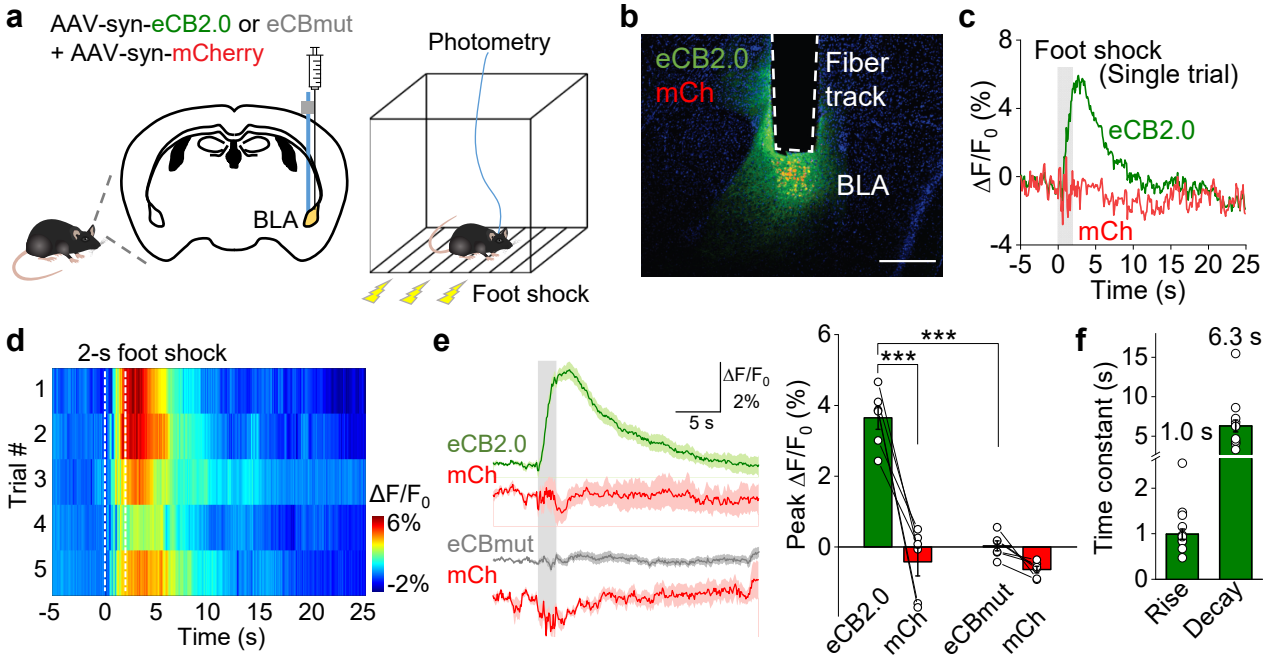

Fig. 5 | Detection of foot shock-evoked eCB signals in the mouse basolateral amygdala

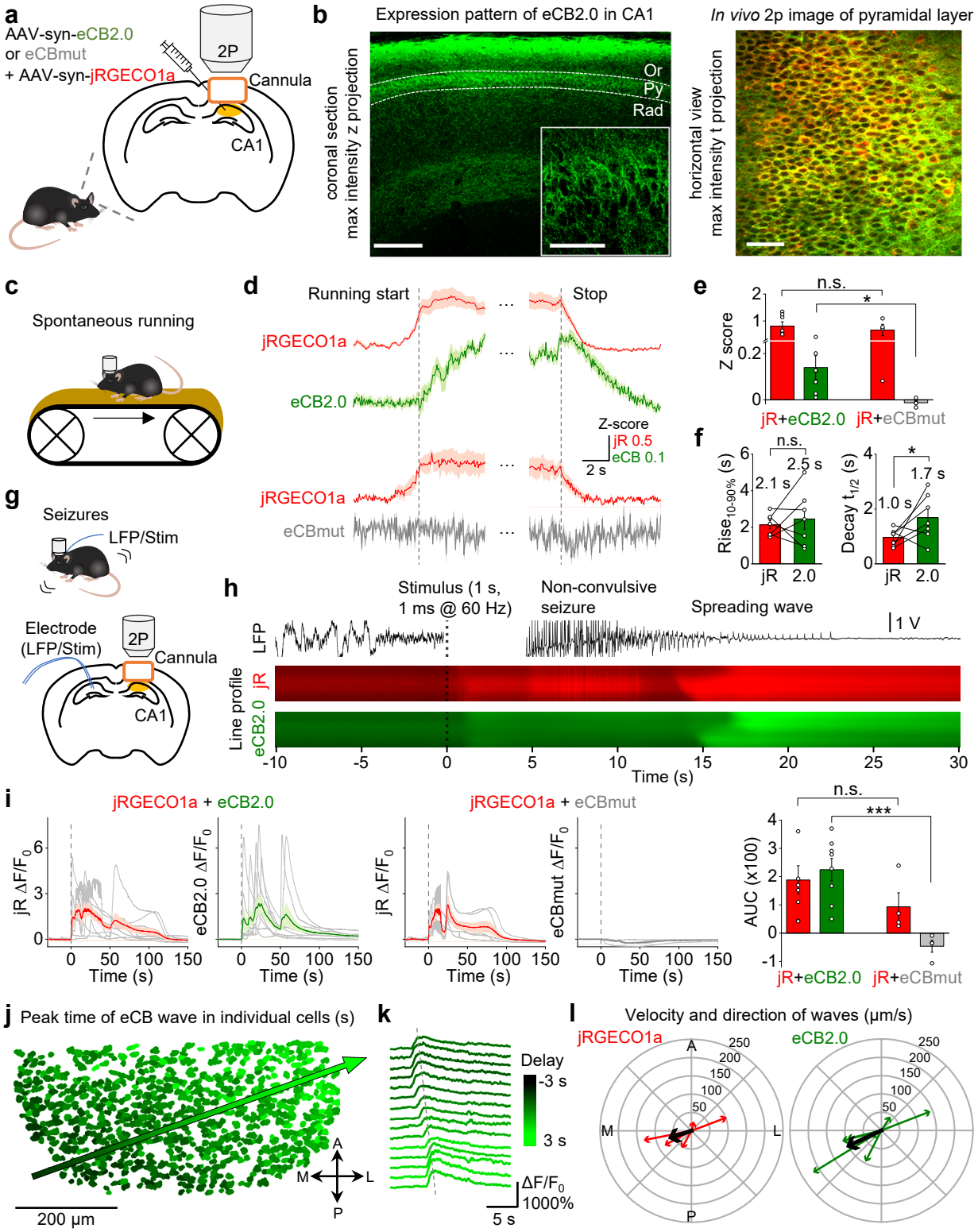

Fig. 6 | Imaging eCB dynamics in mouse hippocampus during running and seizure

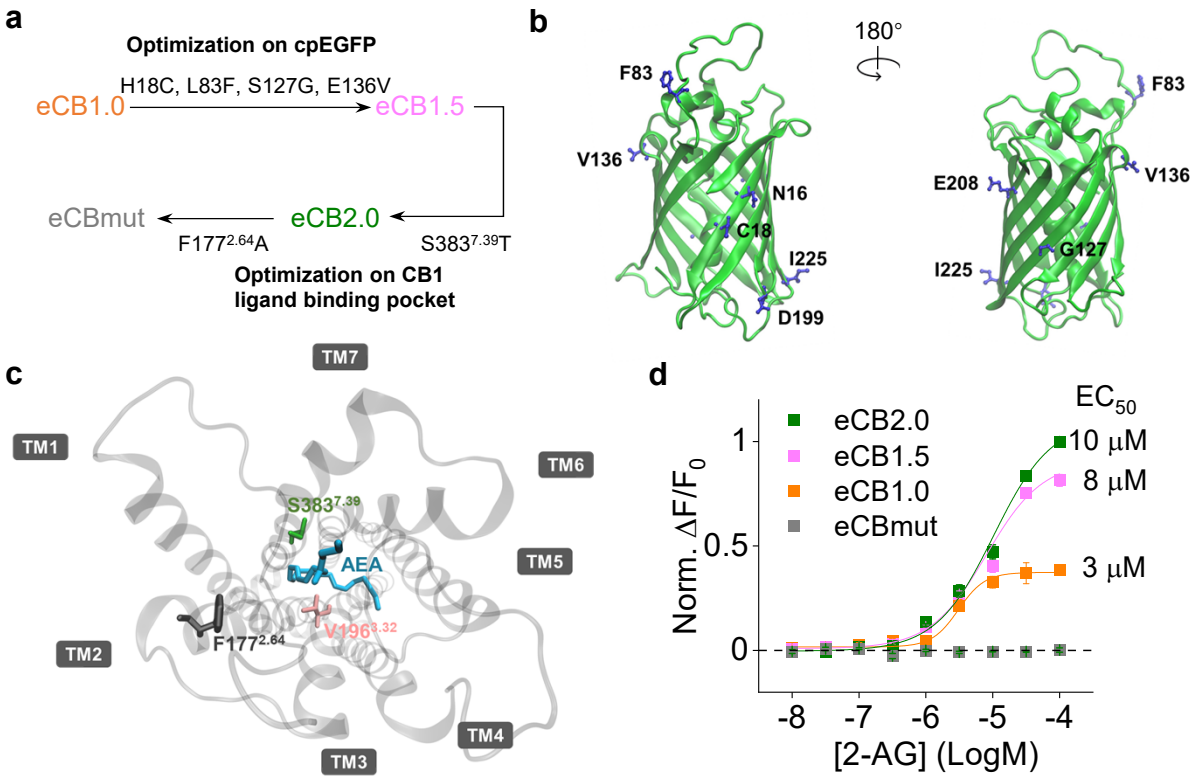

Extended Data Fig. 1 | Evolution of GRAB$_{eCB}$ sensors during the screening

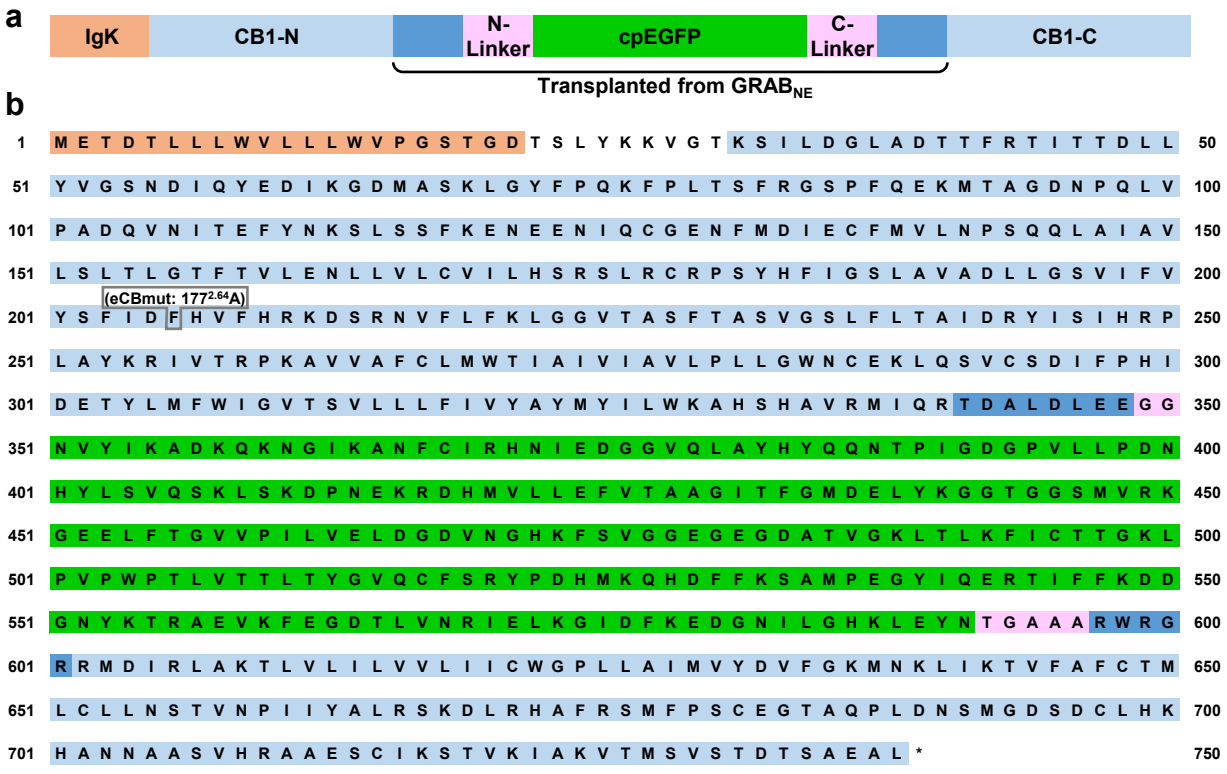

Extended Data Fig. 2 | Full amino acid sequences of eCB2.0 and eCBmut

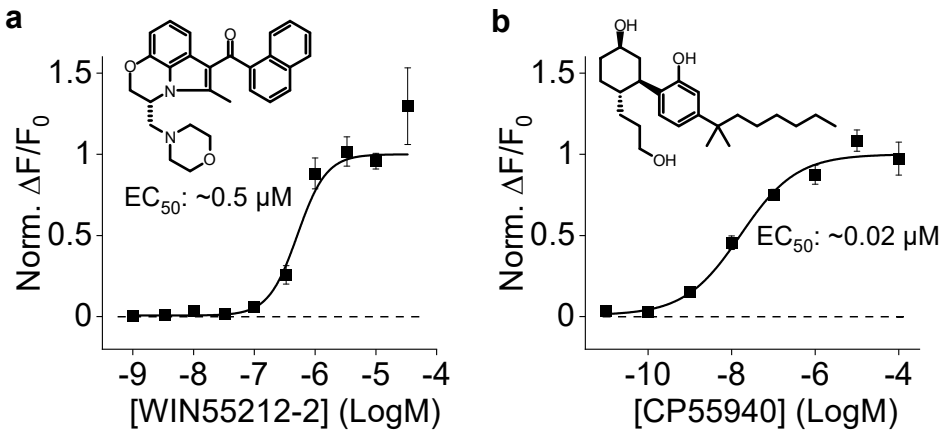

Extended Data Fig. 3 | eCB2.0 responses to synthetic CB1R agonists

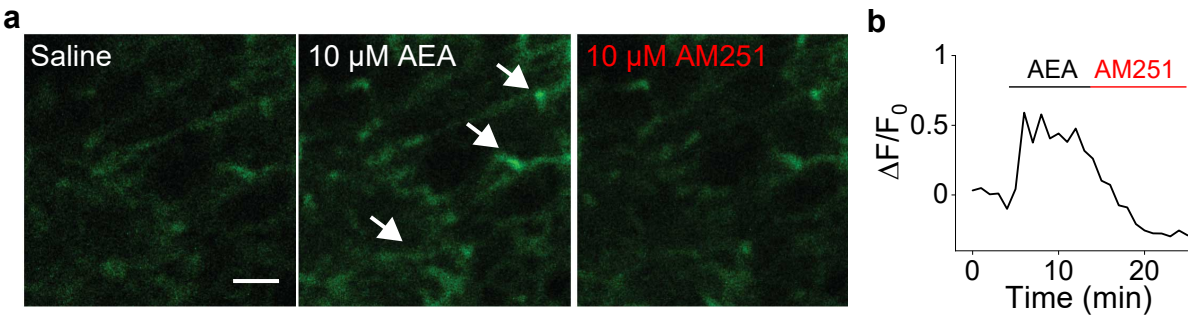

Extended Data Fig. 4 | 2P imaging of eCB2.0 in acute mouse striatal slices

FIGURE LEGENDS

Fig. 1 | Development and characterization of GRAB$_{eCB}$ sensors in HEK293T cells

a, Schematic diagrams depicting the design and principle of the GRAB$_{eCB}$ sensor.

b, Screening steps of GRAB$_{eCB}$ sensors and fluorescence responses to 10 μM 2-AG of GRAB$_{eCB}$ candidates in HEK293T cells. eCBmut was generated by introducing F177$^{2.64}$A to eCB2.0.

c, Expression and fluorescence response to 100 μM 2-AG and AEA of eCB2.0 in HEK293T cells.

d, Dosage dependent responses of eCB2.0 to 2-AG and AEA in HEK293T cells. EC$_{50}$s of 2-AG and AEA were labelled. n = 3 wells.

e, Responses of eCB2.0 to eCBs and varied neurotransmitters and neuromodulators. Note the responses to eCBs were blocked by CB1R inverse agonist AM251. LPA, lysophosphatidic acid; S1P, sphingosine-1-phosphate; ACh, acetylcholine; DA, dopamine; GABA, gamma-aminobutyric acid; Glu, glutamate; Gly, glycine; NE, norepinephrine; 5-HT, 5-hydroxytryptamine; His, histamine; Epi, epinephrine; Ado, adenosine; Tyr, tyramine. n = 3-4 wells.

f, Illustration of a local puff system with a glass pipette filled with 100 μM 2-AG or AM251 placed close to an eCB2.0-expressing cell. Black dash line indicates the scanning region of interest.

g, Line scanning fluorescence responses (left) and summary of on/off time constants (right) of eCB2.0 to 2-AG or AM251. n = 11 (or 4) cells for rise (or decay) kinetics measurement.

h, G protein coupling of CB1R and GRAB$_{eCB}$ sensors measured using a BRET G$_{\beta\gamma}$ sensor. n = 3 repeats.

i, β-arrestin coupling of CB1R and GRAB$_{eCB}$ sensors measured using the Tango assay. n = 3 wells.

Values with error bars indicate mean ± SEM. Student's t test performed; ***p < 0.001. Scale bar in (c) and (h), 30 μm.

874 **Fig. 2 | Characterization of GRAB$_{eCB}$ in primary cultured neurons**
875 **a**, Localization of eCB2.0 in primary cultured rat cortical neurons. eCB2.0 displayed well in
876 neuronal membrane of axons (indicated by arrow-labelled synaptophysin-mScarlet),
877 dendrites and spines (indicated by arrowhead-labelled psd95-mScarlet).
878 **b**, Expression and fluorescence response to 100 μM 2-AG and AEA of eCB2.0 and eCBmut.
879 Insets on eCBmut images are contrast-enhanced to indicate the expression of the sensor.
880 **c**, Dose dependent responses of eCB2.0 and eCBmut in neurites to 2-AG and AEA. n = 3
881 cultures.
882 **d**, Quantification of eCB2.0 responses to 100 μM 2-AG and AEA in neuronal somata and
883 neurites. n = 3 cultures.
884 **e**, Images, trace and quantification of eCB2.0 fluorescence to long-term WIN55212-2
885 application in neurons. n = 3 cultures.
886 Values with error bars indicate mean ± SEM. Student's t test and one-way ANOVA test
887 performed; ***p < 0.001. Scale bar in (a), 30 μm (upper) and 15 μm (lower); in (b), 30 μm;
888 in (e), 100 μm.
889

Fig. 3 | Imaging endogenously released eCBs in primary cultured neurons

a, Expression of R^{ncp}-iGluSnFR and eCB2.0 in neurons, pseudocolor images, and fluorescence traces showing the responses of R-iGluSnFR and eCB2.0 to 100 electrical pulses. 100 white circles (12.4 μm in diameter) indicate ROIs for quantification.

b, Loading of Calbryte590 and expression of eCB2.0 in neurons, pseudocolor images, and fluorescence traces showing the responses of Calbryte590 and eCB2.0 to 100 electrical pulses. 100 white circles (12.4 μm in diameter) indicate ROIs for quantification.

c, Relationship between peak Calbryte590 signals and peak eCB2.0 signals, evoked by 1, 5, 10, 20 electrical pulses and 20 electrical pulses without extracellular Ca^{2+}. Data were normalized to signals evoked by 200 electrical pulses at 50 Hz. n = 4 cultures.

d, Diagram showing the eCB synthesis pathway and the pharmacological perturbation.

e, Representative traces showing the eCB2.0 responses to 20 electrical pulses stimuli before (1) and after DO34 incubation (2), as well as the response to WIN55212-2.

f, Quantification of peak eCB2.0 responses to 20 pulses stimuli before (Ctrl) and after 26 min DO34 incubation (DO), as well as the response to WIN55212-2. n = 3 cultures.

g, Diagram showing the eCB degradation pathway and the pharmacological perturbation.

h, Representative traces showing the eCB2.0 responses to 20 electrical pulses stimuli before (1) and after JZL184 or URB597 incubation (2), as well as after the AM251 incubation.

i, Quantification of decay time constant before (Ctrl) and after 68 min JZL184 (or URB597) incubation (JZL or URB). n = 3 cultures.

j, Pseudocolor images of spontaneous eCB transients, single pulse stimulus evoked eCB signals, and 10μM WIN55212-2 induced eCB2.0 signals.

k, Pseudocolor images of a representative eCB transient event.

l, Traces of the single pulse stimulus evoked eCB signal, spontaneous eCB transient and eCB2.0 signal in the presence of AM251 shown in **k**. Normalized traces with rise time constants are shown on the right.

m, Spatial profile of the eCB transient shown in l (left). Quantification of eCB spontaneous transients FWHM is shown on the right. n = 12 eCB transients.

n, Cumulative eCB transients during 19 min recording in the absence (left) or presence of AM251 (right). Pseudocolor images were calculated as maximum temporal projection subtracting average temporal projection over 19 min.

o, Quantification of eCB transient frequency before (Ctrl) and after AM251 incubation (AM). n = 5 (Ctrl) or 3 (AM) x 10 min.

Values with error bars indicate mean ± SEM. Student's t test performed; *p < 0.05, ***p < 0.001. Scale bar in (a) and (b), 200 μm; in (j) and (n), 100 μm; in (k), 10 μm.

Fig. 4 | Detection of eCBs in acute brain slices

a, Schematic diagrams depicting the viral injection and expression in DLS. Acute slices are prepared for electrical stimulation and photometry recording. Dashed box corresponds to the image in b.

b, The expression of eCB2.0 in DLS and cartoons showing the electrical stimulation and photometry recording.

c, Representative traces showing eCB2.0 fluorescence ($\Delta F/F_0$) increase evoked by electrical stimulation with different stimulation pulses and frequencies.

d, Quantification of peak responses, rise and decay kinetics of electrical stimulation-evoked eCB2.0 signals. n = 6 slices.

e, Representative traces and quantification of peak responses showing eCB2.0 fluorescence ($\Delta F/F_0$) increase evoked by electrical stimulation in control group and in AM251 pre-incubated group. n = 3-4 slices.

f, Schematic diagrams depicting the viral injection and expression in CA1, hippocampus. Acute slices were prepared for stimulation and 2 photon imaging.

g, Expression of eCB2.0 in CA1 and placement of the electrode, and pseudocolor images representing the electrical stimulation evoked eCB2.0 response.

h, Representative traces and quantification of peak responses showing eCB2.0 fluorescence ($\Delta F/F_0$) increase evoked by electrical stimulation with varied stimulation frequencies. n = 5 slices.

i, eCB2.0 fluorescence signal ($\Delta F/F_0$) when bath applying AEA and AM251.

j, Traces showing eCB2.0 fluorescence ($\Delta F/F_0$) increase evoked by electrical stimulation before and after applying AM251.

Values with error bars indicate mean ± SEM. Scale bar in (b), 1 mm; in (g), 100 μm.

Fig. 5 | Detection of foot shock-evoked eCB signals in the mouse basolateral amygdala

a, Schematic diagrams depicting the viral expression, fiber photometry recording and behavior paradigm of the foot shock experiment.

b, Expression of eCB2.0 (green) and mCherry (red) in the BLA and placement of the recording; the nuclei were counterstained with DAPI (blue).

c, Representative single trial traces showing eCB2.0 and mCherry fluorescence ($\Delta F/F_0$) during an electrical foot shock.

d, Pseudocolor fluorescence responses of eCB2.0 to the foot shock. Five consecutive trials from one mouse were recorded and plotted relative to the onset of each stimulus.

e, Averaged traces showing eCB2.0 and mCherry (top) or eCBmut and mCherry (bottom) fluorescence during an electrical foot shock (left). Group summary of peak responses is shown on the right. n = 6 mice.

f, Quantification of rise and decay kinetics of foot shock-evoked eCB2.0 signals. n = 21 (or 18) trials from 6 animals for rise (or decay) kinetics quantification.

Values with error bars indicate mean ± SEM. Student's t test performed; ***p < 0.001. Scale bar in (b), 300 μm.

Fig. 6 | Imaging eCB dynamics in mouse hippocampus during running and seizure

a, Schematic diagrams depicting the viral expression and cannula placement.

b, Histology showing the expression of eCB2.0 in CA1 (left) and *in vivo* 2-photon image of pyramidal layer (right) showing the expression of eCB2.0 (green) and jRGECO1a (red).

c, Schematic illustration of the experiment in which mice expressing eCB2.0 and jRGECO1a in CA1 are placed on a treadmill. The fluorescence is recorded using 2-photon microscope.

d, Averaged traces of calcium and eCB transients recorded from somata of individual neurons in the pyramidal layer (left). Plots show the event-triggered average upon the start and stop of spontaneous running episodes (dashed lines).

e, Group summary of peak responses in panel **d**. n = 8 mice for eCB2.0 group and 4 mice for eCBmut group.

f, Quantification data of rise and decay kinetics of jRGECO1a and eCB2.0 signals during running start and stop.

g, Schematic illustration of the electrode placement and experiment in which mice expressing eCB2.0 and jRGECO1a in CA1 are recorded when inducing a kindling seizure.

h, Example trace of LFP, with medio-lateral projections (line profile) of eCB2.0 and jRGECO1a fluorescence during electrically induced non-convulsive seizures and the following spreading wave. Dashed line indicates the stimulus onset.

i, Individual and averaged traces of eCB2.0 (or eCBmut) and jRGECO1a fluorescence signals during the seizure. Dashed line indicates the stimulus onset. Group summary of AUC is shown on the right. n = 8 mice for eCB2.0 group and 4 mice for eCBmut group.

j, Spreading of eCB2.0 signal after a seizure. ROIs representing individual neurons are pseudo-colored according to the peak time of eCB2.0 signal relative to the peak time of the average signal (left). The symbols stand for (clockwise): anterior, lateral, posterior, medial.

k, eCB2.0 traces of individual cells sampled systematically along a line fitted to the spreading wave (arrow). The dashed line shows the spreading of peak signals.

l, Velocity and direction of the spreading eCB and calcium waves. Colored lines show individual sessions. Black lines show the average. n = 7 sessions from 6 mice.

Values with error bars indicate mean ± SEM. Student's t test performed; *p < 0.05, ***p < 0.001, and n.s., not significant. Scale bar in (b, from left to right), 200, 50 and 50 μm.

Extended Data Fig. 1 | Evolution of GRAB$_{eCB}$ sensors during the screening

a, Schematic representation of the evolution of GRAB$_{eCB}$ sensors.

b, 8 sites selected for optimization on cpEGFP.

c, 3 sites selected for optimization on the GPCR ligand binding pocket.

d, Normalized dose-dependent responses of eCB1.0, eCB1.5, eCB2.0 and eCBmut to 2-AG in HEK293T cells. n = 3 wells.

Values with error bars indicate mean ± SEM.

Extended Data Fig. 2 | Full amino acid sequences of eCB2.0 and eCBmut

a, Schematic representation of the eCB2.0 structure.

b, Amino acids sequence of the eCB2.0. $177^{2.64}$ (labelled by the gray box) is mutated to A in eCBmut.

Extended Data Fig. 3 | eCB2.0 responses to synthetic CB1R agonists

a, Normalized dose-dependent responses of eCB2.0 to WIN55212-2.

b, Normalized dose-dependent responses of eCB2.0 to CP55940.

Extended Data Fig. 4 | 2P imaging of eCB2.0 in acute mouse striatal slices

a, 2P images of eCB2.0 (indicated by arrows) expressed in mouse striatum in saline, 10 μM AEA and 10 μM AM251.

b, eCB2.0 fluorescence signal ($\Delta F/F_0$) when bath applying AEA and AM251.

Scale bar, 10 μm.

Extended Data Movie 1 | eCB and calcium signals in mouse hippocampal CA1 during kindling seizure

2P imaging of eCB and calcium signals using eCB2.0 and jRGECO1a in mouse hippocampal CA1 during kindling seizure. LFP was simultaneously recorded to indicate the electrical stimulation and seizure.

Scale bar, 50 μm for images and 1 V for LFP.